CHEMICAL EFFECTS IN EXTERNAL HYPERSONIC FLOWS

Roberto Vaglio-Laurin[1] and Martin H. Bloom[2]

Polytechnic Institute of Brooklyn, Brooklyn, New York

ABSTRACT

This paper[3] gives an account of advances and problems in the area of chemically reacting continua. Emphasis is placed on the discussion of external flows about axisymmetric hypersonic vehicles at zero incidence. Several facets of the problem are treated; in particular: 1) An analysis and correlation of numerical results for complete inviscid flows assuming that either chemical equilibrium or composition frozen at post-shock equilibrium conditions is presented. 2) An assessment of behavior and effects of rate processes is performed by means of one-dimensional calculations along streamlines. On this basis it is shown that the latter calculations and the frozen model may be used in tandem to obtain reasonably accurate estimates of observables in practical situations. 3) The behavior of non-equilibrium boundary layers over bodies is discussed. 4) A quantitative study of wakes, considering the influence of shock induced vorticity and of inner core, is presented for both laminar and turbulent flows.

INTRODUCTION

Detailed knowledge of chemical effects in hypersonic flows is of scientific and practical interest, as it bears upon communications, diagnostics, etc. Analyses have usually involved a combination of continuum fluid mechanics with classical chemical kinetics and statistical mechanics for mixtures of perfect

Presented at ARS International Hypersonics Conference, Cambridge, Massachusetts, August 16-18, 1961; this research was carried out under the sponsorship of Contract no. AF 49(638)-217, Project no. 9781, monitored by the Air Force Office of Scientific Research, USAF.

[1]Research Professor, Dept. of Aerospace Engineering.

[2]Professor, Dept. of Aerospace Engineering.

[3]This paper represents a condensed version of Ref. 1.

gases. To simplify the obviously complex problem, partially uncoupled flow models have been devised; for example, chemical rate processes have been studied within one-dimensional approximations, often in combination with simplified thermodynamic descriptions.

In this spirit, the authors attempt to develop reasonably simple rules for evaluation of observables; attention is directed toward flows over blunt nosed slender bodies in flight regimes where distinct discontinuity (shock) surfaces and separate regions of inviscid and viscous flow can be recognized. The following problem areas are dealt with:

1) Determination of the inviscid flow field about blunt nosed slender bodies at zero incidence for flight in air and conditions wherein departures from thermal equilibrium occur (see the next section). In this connection a complete correlation is instituted of pressures on bodies, of shock shapes, and of transversal distribution of flow properties, using a model justified by rate calculations along streamlines. In turn direct combination of the forementioned model and calculations permits relatively simple estimates of observables in the flow field.

2) An assessment of behavior and effects of rate processes in inviscid flows about blunted slender bodies under various flight conditions (see the third section). Here some trends are pointed out on the basis of one-dimensional rate calculations; validity of the latter is assessed in turn.

3) A quantitative study of wakes behind axisymmetric hypersonic vehicles, considering influence of shock induced vorticity and of inner core for laminar and turbulent flow (see the fourth section). In this connection the authors postulate situations and examine ensuing effects; conditions for stability, transition and persistence of turbulence are not treated.

4) A qualitative assessment of nonequilibrium boundary layers over bodies, with emphasis on situations characterized by a cold noncatalytic wall; also estimates of viscous-inviscid interactions and their effects on rate processes in the external flow (see the fifth section).

5) Order of magnitude evaluation of wake unsteadiness and heat loss by radiation (see the sixth section)

Clearly, quantitative effects due to three-dimensionality, low density, contamination, etc. require future consideration.

INVISCID FLOW FIELDS

Emphasis is given to flows about blunt nosed slender bodies; in particular the authors report on configurations with long cylindrical afterbodies representative of viscous wakes.

Current investigations of the observables and physical state involve one-dimensional rate calculations along streamlines with a prescribed distribution of one flow property, e.g., either pressure (Ref. 15) or mass flow per unit area (Ref. 16). The latter is determined from n -dimensional fluid mechanical analysis based on a simplified gas behavior (e.g., thermodynamic equilibrium). The qualitative behavior of the actual flow and the accuracy of the aforementioned studies are assessed here.

Flow fields about blunt nosed slender bodies can roughly be divided into two regions: the nose proper, and the afterbody and wake. Chemical effects in the nose region have been studied by Freeman (Ref. 2) and Lick (Ref. 4). The Newtonian approach (Ref. 2) readily shows that in the region of very strong shock (where the local velocity is either subsonic or low supersonic) the pressure on the body is not affected to a first approximation by finite-rate chemical reactions. Lick's detailed numerical results confirm the smallness of this effect. Though shock detachment distances and local density and temperature of the gas depend strongly on the actual rate processes, the shock shape, the pressure field (in particular, pressure distributions along streamlines), and the general fluid mechanical aspects of the problem are not affected substantially. Thus, one-dimensional calculations, as mentioned in the foregoing, can yield rather accurate predictions for local values of species concentrations; naturally, more detailed analysis is required when gradients of concentrations (e.g., for electrons) are of interest.

The situation changes beyond the sonic point on the body where the Newtonian solutions have a singular behavior. Unfortunately there is a lack of a simple but accurate theoretical description of this region even for ideal gas flows; Freeman's results (Ref. 3) for a sphere show a dependence near the singular point on $\epsilon^{3/11} = [(\gamma - 1)/(\gamma + 1)]^{3/11}$ rather than on ϵ, and $\epsilon^{3/11}$ is never small enough in actual flows for a Newtonian-detached free layer theory to hold. The difficulty has been bypassed in practice by use of semiempirical laws for simple body shapes (such as modified Newtonian plus Prandtl-Meyer expansion for quasi-spherical configurations). Sufficient information is not available at the present time to establish similar thumb rules for general situations; also, it is recognized that empirical approaches will have practical usefulness only

if rate processes along individual streamlines prove to be rather insensitive to the details of pressure distribution along the same. The present authors' preliminary results (Ref. 1) indicate that pressure distributions in the shoulder region are sizably affected by the actual thermodynamic behavior of the gas; however, estimates thereof are possible and need not be extremely accurate for the purpose of calculating rate processes along streamlines. Extensive investigations seem in order.

Chemical freeze also has a sizable influence on pressure distributions over slightly blunted noses, such as the configuration b (Fig. 2). Numerical results (Ref. 1) show that the magnitudes of overexpansion and of subsequent recompression overshoot increase with the percent of energy frozen in the flow. In fact, the freeze brings about a substantial diminution of effective nose drag (hence the larger overexpansion in the initial region where the nose influence is dominant) and, in contrast, an increased lateral impulse for a given rate of expansion of the body cross section (cone angle).

The afterbody region is now considered; this is of particular interest of detection, diagnostics, etc. A few investigations (Refs. 5, 6 and 7), all assuming thermodynamic equilibrium of standard air, have been carried out in this area. The present analysis takes into account prior indications of substantial freezing of major air components in the upstream regions of the shock layer under typical flight conditions above 125 kft. A simplified model, shown in Fig. 1a, assumes chemical freeze above A B and beyond the shock segment B C (line A B is a second family characteristic intersection the body just downstream of the sonic point); chemical equilibrium is assumed in region O B A B and directly behind B C. Use of this model is verified a posteriori. The air here is composed of N, N_2, O, O_2, N O in vibrational equilibrium. Table 1 and Fig. 2 show flight conditions and nose shapes for which calculations were made. The calculation procedure is outlined in Ref. 1.

A brief review and extension of available information related to flows over blunted slender bodies is in order before proceeding to the study of numerical results. Most of the work in this area has dealt with an asymptotic model wherein the effect of bluntness is replaced by a concentrated force acting at the nose; the hypersonic equivalence principle then permits reduction of the problem to the corresponding unsteady situation for which classes of similar solutions exist. The range of validity of the analogy is not clearly defined, particularly in its dependence on several underlying approximations; among these are:

1) The solution is of an asymptotic nature; thus, the origin

of the coordinate system is unknown a priori.

2) Strict similarity can only be established for a perfect gas with constant specific heats.[4]

3) Even for perfect gas flows the equivalence principle breaks down in the high entropy layer near the body.

4) Details of nose shape, which are essential in determining the characteristics of the entropy layer, are neglected.

The equivalence principle and the similitude suggested by Cheng (Ref. 5) for equilibrium flows provide a description of the entire field only at stations where the lateral extent of the singular layer adjacent to the body is small in comparison with the lateral extent of the field. Such is the case for extremely large values of the longitudinal coordinate x (made dimensionless with respect to the radius of the nose base); at smaller distances from the nose data must be interpreted and correlated on the basis of a two-layers model with the inner layer characterized by constant pressure and the outer by small perturbations of the hypersonic free stream (Refs. 7 and 8). The considerations of Cheng are strictly applicable to the outer layer; correspondingly, tangency conditions at the surface of the body should be replaced by compatibility conditions at the boundary between the two layers. Consideration is now given to the particular case of flow over a blunted plate or cylinder and ideally replace the dividing streamline with a solid boundary described, case by case, by an appropriate equation $y_{sl}(x)$. One may denote by τ the maximum slope of the streamline; also, a reference length is introduced

$$L = M_\infty^{(3+j)/(1+j)} C_D^{1/(1+j)} R \tag{1}$$

where $j = \begin{cases} 0 \\ 1 \end{cases}$ for two-dimensional and axisymmetric flow, respectively, and C_D is the drag coefficient of the nose. For a given shape of the dividing streamline, all flow properties [pressure p/p_∞, density ρ/ρ_∞, velocities $u/\tau^2 U_\infty$ and $v/\tau U_\infty$, enthalpy h/h_∞, species concentrations X_i, etc.] in the outer layer exhibit a functional dependence of the type

$$p/p_\infty = f\left[\frac{x-x_*}{L}, \frac{y-y_*}{\tau L}, M_\infty \tau, p_\infty, \rho_\infty, X_{i\infty}\right] \tag{2a}$$

[4] The requirement can be made somewhat less restrictive for constant energy solutions where it is sufficient that the internal energy be expressible as the product of pressure times a function of the density (Ref. 9).

where x_* , y_* are, for example, the coordinates of the point of intersection between dividing streamline and shock. Similarly the equation of the shock surface takes the form

$$(y_{sh} - y_*)/rL = \bar{\delta}\left[\frac{x - x_*}{L},\ M_\infty r,\ p_\infty,\ \rho_\infty,\ X_{i\infty}\right] \tag{3a}$$

If attention is now limited to the region within which bluntness effects become practically negligible (say $x \leq 50R$) one finds there $(x - x_*)/L << 1$, $(y - y_*)/rL << 1$. Under these conditions flow properties in the outer layer and shock shapes can be described by power series like

$$p/p_\infty \cong \left(\frac{x - x_o}{L}\right)^{\ell_1}\left(\frac{y - y_o}{rL}\right)^{k_1} f_1(M_\infty r, p_\infty, \rho_\infty, X_{i\infty}) + 0\left[\left(\frac{x - x_o}{L}\right)^{\ell_2}\left(\frac{y - y_o}{rL}\right)^{k_2}\right] + \ldots \tag{2b}$$

and

$$(y_{sh} - y_*)/rL = \text{constant} + \left(\frac{x - x_o}{L}\right)^{m_1} \bar{\delta}_1(M_\infty r, p_\infty, \rho_\infty, X_{i\infty}) + 0\left[\left(\frac{x - x_o}{L}\right)^{m_2}\right] + \ldots \tag{3b}$$

where $(x_o - x_*)$ and $(y_o - y_*)/r$ are quantities $O(1)$, $(\ell_2 + k_2) > (\ell_1 + k_1)$, $m_2 > m$. Naturally the exponents k through m can be functions of the particular streamline shape and, therefore, of nose configuration and drag coefficient; thus, hypersonic flows over blunt nosed flat plates or cylinders are not strictly similar. For each nose shape and dividing streamline there are related shock shapes and distributions of flow properties in the outer layer. A study of numerical (Refs. 1 and 7) and experimental (Ref. 10) results shows that the range of small perturbations can include only shocks weaker than 20 deg, the dividing streamline is determined correspondingly. For velocities up to the orbital value and for altitudes below 300,000 ft, transition across a 20 deg shock involves negligible dissociation of the air; the functions f_1 and $\bar{\delta}_1$ in Eqs. 2b and 3b can then be reduced to the form $f_1(M_\infty r, \bar{\gamma})$, $\bar{\gamma}$ being a representative value of the isentropic exponent for the gas in the outer layer.

The foregoing conclusions can readily be extended to the asymptotic behavior of flows about blunted plates and cylinders involving departures from chemical equilibrium and, subsequently, freeze of the composition downstream of a certain station; it has already pointed out that this is the case for hypersonic flight of typical vehicles[5] at altitudes in excess of about

[5]The authors denote as typical a nose having a base radius of 1 ft; the boundary of freeze becomes lower as that radius becomes smaller.

120,000 ft. The extension follows readily from considerations of momentum and energy flux across a control surface enclosing a portion of the body (surface ABCDOA in Fig. 1b); these result in the integral relation (for a flat plate or cylindrical afterbody)

$$D_n - \int_{y_b}^{y_{sh}} \rho h_d (2\pi y)^j \, dy = \int_{y_b}^{y_{sh}} \rho \left(\frac{v^2}{2} + e_t \right) (2\pi y)^j \, dy \qquad (4)$$

where D_n denotes the pressure drag of the nose, h_d represents the energy of dissociation per unit mass frozen into the gas, and e_t the thermal (internal) energy of the gas. If the composition of the gas (or its major constituents becomes frozen along the line PQ (see Fig. 1b), and no further dissociation takes place behind the shock QC, the second term at the left-hand side of Fig. 4 becomes a constant (within the hypersonic approximation); a fictitious drag $\overline{D}_n$ and drag coefficient $\overline{C}_D$ can be defined

$$\overline{C}_D = \left[\frac{1}{2} \rho_\infty U_\infty^2 (\pi R)^j R \right]^{-1} \left[D_n - \int_{y_b}^{y_{sh}} \rho h_d (2\pi y)^j \, dy \right] \qquad (5)$$

The situation is then equivalent to that encountered in an equilibrium flow with a more slender nose having drag $\overline{D}_n$. Naturally, the equivalence prevails only downstream of the characteristic QR through the point Q. Analysis of numerical results bears out the above point of view and provides rules for simple estimates in practical situations (Ref. 1).

Computed pressure distributions for different nose shapes are plotted in Figs. 3, 4 and 5. Several comparative features are readily apparent, namely:

1) Departures from thermal equilibrium induce a faster decay of the pressure. The difference between equilibrium and frozen results increases as the dissociation energy bound in the gas becomes a larger fraction of the work done by the pressure drag of the nose. The high drag cone of Fig. 5 offers a particularly dramatic example in this connection.

2) For a given configuration losses and ensuing effects on pressure distributions depend more strongly on flight velocity rather than on altitude (Fig. 3); this behavior is readily justified by inspection of Fig. 6.

3) Distributions on afterbodies having nonspherical noses are characterized by local recompressions at stations somewhat downstream of the shoulder; asymptotic behavior is attained only beyond these stations.

4) Effects of nose shape and of nonsimilar distribution of energy in the transverse flow field at the shoulder are also evidenced (Ref. 1). For example, configurations with blunted conical noses exhibit a very rapid decay of pressure in the region between the shoulder and the recompression station. The bulk of this effect depends on the relatively small thickness of the shock layer at the shoulder. In fact, it is known that, in self-similar solutions, the rate of growth of the shock depends weakly on the drag coefficient ($\approx C_D^{1/4}$) whereas the energy in the transverse flow field is proportional to C_D; the latter changes greatly with nose configuration and represents the dominant influence for the decay. Also, it is known that shock layer thickness and distribution of energy encountered at the shoulder on a spherical nose are quite close to those required for a self-similar solution and, indeed, produce a pressure decay consistent with approximate blast predictions. For bodies with conical noses where the thickness of the shock layer is substantially different from that observed on a sphere, one should then stretch the longitudinal coordinate approximately in the ratio of the thicknesses CD/AB as shown in Fig. 4. When this is done the blast theory yields predictions ($p/p_\infty = .405 + [AM_\infty^2 C_D^{1/2}/(x+\xi)][AB/CD]$) that are reasonably close to reality (points shown in Fig. 4).

Satisfactory correlation of the asymptotic pressure distributions (Fig. 7) is provided by a blast equation modified in accord with the formal solution (Eqs. 2b and 3b), namely

$$(p/p_\infty - C)^{2(1-m)} = A(\gamma)\frac{M_\infty^2 \overline{C}_D^{1/2}}{x+\xi} \qquad (6)$$

where m is the exponent in the equation of the shock, $\overline{C}_D$ the drag coefficient defined by Eq. (5), and ξ an appropriate origin of coordinates chosen (consistently with the asymptotic nature of the solution) so to match the value of pressure at the station $x = \bar{x}$ where the self-similar behavior is first attained. In Eq. 6 one may represent the effect of second order corrections to the solution by the constant C, and the effect of gas behavior by the function $A(\gamma)$ taking γ constant and equal to the value computed at the intersection between shock and dividing streamline. Therefore, in absence of specific information for the quantities A and C, the values pertaining to the classical blast solution are applied.

The region of similar asymptotic behavior for the model frozen flows is bounded by the second family characteristic line that originates at the shock point where gas dissociation is last observed. The flow upstream of this line lacks similarity in the distribution of energy associated with the transverse flow field; the situation, as manifested in pressure distributions and shock shapes, arises from the low effective energy of the gas flowing near the body (where the dissociation is large) as opposed to that of the gas flowing through weaker portions of the shock. Since the energy is proportional to the drag of the nose, the pressure has a very rapid local decay near the shoulder.

A complete description of the flow field requires that bow waves and transverse distributions of flow properties be also known. For given configuration and flight conditions, the shock pertaining to frozen flow is at first closer to, and then farther away from the body, as compared with the shock for equilibrium flow. The situation is easily explained by the different growth of the entropy layer and different shape of the dividing streamline in the two cases. As pointed out previously the two classes of flows are not strictly similar; in particular, the leading term of the laws for the corresponding shock surfaces (Eq. 3b have exponents that depend on nose configuration and drag coefficient. This point of view is borne out by Van Hise's (Ref. 12) and the results in Ref. 7 for perfect gas and equilibrium air. Inspection of Fig. 14 of Ref. 12 (for example, cases B-4 and D-2), and Fig. 15, of Ref. 7 shows that the exponent of the shock law increases as the drag coefficient decreases. Reduction of the effective drag coefficient by chemical freeze leads to exactly the same effect; this is shown in Fig. 8 for all configurations on hand. Here all cases have been correlated in terms of the equation

$$y - y_o = B(\gamma)\,\bar{C}_D^{1/4}\,(x - x_o)^m \qquad (7)$$

with $y_o = 0.4$, $x_o = (x_s - 1.0)$, x_s being the abscissa of the shoulder, m a function of drag coefficient and nose shape, and $B(\gamma)$ a function taken from standard blast theory (Ref. 1). For each particular flight condition and gas behavior γ has been set equal to the value computed at the intersection between shock and dividing streamline.

Consistent with the similarity of pressure decays and of shock shapes, as manifested by the foregiven correlations, distributions of flow properties in the outer layer should also be similar; even more, Eq. 2b indicates that identical distributions should be obtained for different configurations provided

the associated values of the exponent m are the same.[6] This point of view is shown by the diagrams in Fig. 9. The formal solution 2b suggests the correlation

$$\frac{p_{sh}-p}{p_{sh}-p_{sl}} = 1-\left(\frac{y-y_{sl}}{y_{sh}-y_{sl}}\right)^{k} \tag{8}$$

where $y_{sl}=y_o+O(r)=y_o$ denotes the ordinate of the streamline at a general station x, and k is a quantity uniquely related to the exponent m of Eq. 7 and, like the latter, contingent with the particular configuration on hand. Incidentally, the quality of the correlations in Fig. 9 also indicates a reasonable accuracy of the calculations.

With frozen flow and known shock shape, two thermodynamic properties (p and ρ) and mass flow are sufficient to determine the local state of the gas.[7] The two layers model, together with the correlations 7 and 8, then provide sufficient information for carrying out preliminary estimates (Ref. 1) on the asymptotic behavior of inviscid flow fields about blunted cylinders; these are of interest for diagnostics thereof and as inputs for wake calculations. At this stage one may wish to substantiate the frozen model on which the present considerations are based and to review a few representative results of rate calculations along streamlines within the flow fields of interest here. These are the topics of the following section.

SOME EFFECTS OF RATE PROCESSES

This section sets forth an evaluation of chemical and electron effects contingent with rate processes in the shock layer. The purpose is threefold, namely: To assess generally the behavior of rate processes under various flight situations and to determine conditions under which either equilibrium or frozen flow are encountered; to establish the sensitivity of rate calculations to prescribed pressure distributions; and to substantiate the model used for the inviscid flow analysis of the second section.

Detailed analysis of the shock structure (Ref. 13) has verified the Von Neumann model which postulates nonrelaxing transition of pressure and temperature followed by chemical relaxation (Fig. 10). The further studies here employ detailed and realistic

[6] Identical values of m (Fig. 8) pertain, for example, to equilibrium flows about low drag noses and to frozen flows about spherical noses.

[7] Electron concentrations may require special attention as discussed in the third section.

rate-chemistry calculations along streamlines in the shock layer starting with the chemical relaxations directly behind the "pressure-shock". Pressure distributions as obtained in the section on inviscid flow fields under the assumptions of either equilibrium or frozen gas composition[8] have been imposed. The gas has been assumed to have a basic composition in mass fractions of 0.2337 oxygen, 0.7663 nitrogen, and to dissociate into a mixture involving seven chemical species, namely, N, N_2, O, O_2, NO, NO^+, e^- which partake in the following reactions

$$N_2 + X \rightleftharpoons 2N + X \tag{9a}$$

$$O_2 + X \rightleftharpoons 2O + X \tag{9b}$$

$$N_2 + O_2 \rightleftharpoons 2NO \tag{9c}$$

$$NO + X \rightleftharpoons N + O + X \tag{9d}$$

$$NO + X \rightleftharpoons NO^+ + e^- + X \tag{9e}$$

$$N + O \rightleftharpoons NO^+ + e^- \tag{9f}$$

$$N_2 + O \rightleftharpoons NO + N \tag{9g}$$

$$NO + O \rightleftharpoons O_2 + N \tag{9h}$$

The individual components behave as thermally perfect gases, individually in thermal equilibrium, although they may engage in dissociative reactions. Rate parameters have been selected in accord with the estimates (based on both theory and experiment) of Ref. 14; where different catalysts X are indicated, each (or each group) has been treated in a separate reaction and the corresponding rate parameter applied. No direct information was available on the rate parameter for reaction 9e; this has been taken equal to that of Eq. 9b.

Study of even a limited number of cases exhibits several

[8] At least for the configurations analyzed here, nonequilibrium pressure distributions should be intermediate between the two considered limits.

interesting features. In Fig. 11 are presented results of calculations along a body streamline for a sphere-cylinder combination with nose radius of 1 ft, flight velocity of 23,000 fps at altitudes of 150,000 and 124,000 ft, and two pressure distributions, respectively pertaining to flow in thermal equilibrium and flow frozen near sonic velocity (model in the second section). Inspection of the diagrams shows that, in all three cases considered, oxygen and nitrogen recombination freezes near the sonic velocity, whereas the ionization reaction departs from equilibrium (but does not freeze) shortly thereafter. The behavior of the latter is evidenced by comparison of the actual distribution of electron density against those that would prevail if: 1) General freeze would onset simultaneously for recombination of neutral and charged particles (curve $n_e^* \rho/\rho^*$, with * denoting values at the station $\tilde{s} = 1$ where nitrogen freezes); 2) the ionization were in equilibrium with the local (frozen) concentrations of atomic oxygen and nitrogen (identified by isolated points $\odot$). It is seen that the actual situation is intermediate between those two extremes; also there is a stronger tendency to approach local equilibrium at the lower altitude (124,000 ft). Comparison of results pertaining to the two pressure distributions (for equilibrium and frozen flow, respectively) at the 150,000 ft altitude demonstrates the insensitivity of rate processes to the details of those distributions.

A behavior quite similar to that just described can be observed along a streamline intersecting the shock near the sonic point. The situation changes substantially when a streamline is considered that intersects weaker portions of the shock. Figure 12 presents results for the particular case of 30 deg deflection at the wave front. Configuration and flight velocity are the same as considered in the foregoing. It is readily apparent from the plots that partial dissociation of the gas takes place over a rather extended initial region (approximately 1-ft long), and that all reactions become practically frozen thereafter; however, peaks of dissociation and ionization are much below the values that would be attained if the gas were frozen in its ideal equilibrium composition downstream of the shock (* denote such conditions). The behavior is contingent with the long relaxation distance behind a relatively weak discontinuity and with the overlapping streamwise decay of pressure in the actual flow field.

The results for the various streamlines evidence the existence of two regions with the flow fields of interst for

altitudes in excess of about 110,000 ft.[9] One region is characterized by relaxation distances for dissociation small compared with a typical nose dimension, and includes the fluid that crosses the strong shock; the other is characterized by large streamwise changes in pressure over the relaxation distance, and involves the remainder of the gas which undergoes dissociation. The flow within the first region initially appraches local equilibrium; subsequently atomic recombination there freezes (at some station determined by altitude, flight velocity, typical dimension and nose shape in order of importance), while recombination of ions and electrons persists, though at a rate insufficient to maintain local equilibrium with the given (frozen) concentrations of atomic oxygen and nitrogen. In contrast, the flow within the second region does not attain local equilibrium at any station; the rate processes there, and the contingent peak values of dissociation and ionization attained prior to the onset of freeze, are governed by a strong interplay between driving conditions for dissociation (as determined by initial flow properties) and the damping effect of expansion and temperature decrease. Available information on relaxation distances behind plane shocks must then be used judiciously; in fact, it appears desirable to investigate quantitatively the relative importance (so far as gas behavior is concerned) of the latter ideal distances as opposed to lengths like R (radius of curvature of the shock) or $\left(\frac{1}{p}\frac{dp}{ds}\right)^{-1}$ that characterize the streamwise pressure gradient behind the shock.

The situation, though delicate, does not obliterate the validity and usefulness of the models suggested in this paper. According to the present results the "frozen" model of the second section yields a conservative estimate for the amount of dissociation in the flow, and therefore, for the accompanying effects on observables. The insensitivity of rate processes to details of pressure distribution corroborates the one-dimensional approach to their determination; the ensuing results can, in turn, be used to generate more accurate estimates of the actual flow pattern (at least asymptotically).

Here the authors terminate their considerations of chemical effects in inviscid hypersonic flows, and turn attention to regions of the flow where transport phenomena are important;

---

[9]Again, reference is made to typical nose dimensions of about 1 ft; if these are sharply reduced (say by orders of magnitude as in the case of firing range models) the first region may disappear.

this is the object of the following sections.

WAKE REGION

Basic features of the flow behind blunt based bodies at supersonic speeds (see Fig. 13) have been appreciated for several years (e.g., Chapman, Ref. 17). The shed boundary layer passes into the central core, which necks down to about a body radius for usual blunt bodies, and may be laminar or turbulent. The shock induced outer portion of the wake is laminar initially. When the core and outer wake are both laminar or both turbulent, the characteristic diffusive dimension δ_c is the bow-shock radius. One may note the following useful relations between body drag D, momentum loss integral θ_c, drag coefficient C_D, and the viscous layer radius δ_c, namely: $D/2\pi = \rho_e u_e^2 \theta_c = \int_0^{\delta_c} \rho u (u_e - u)\, y\, dy \sim \rho_e u_e^2 \delta_c^2 \quad (u_e - u_{oc})$, so that $\theta_c^{1/2} \simeq \delta_c/2$, and $\theta_c = C_D r_n^2/4$, where $C_D = D/(\rho_e u_e^2/2)(\pi r_n^2)$, r_n is the nose radius, ρ is density, u is axial velocity, subscript e denotes outer edge values and subscript c constant values at an initial station.

Laminar diffusion times are of order $\delta_c^2 \rho/\mu$ or $\theta_c \rho/\mu$, where μ/ρ is a representative kinematic viscosity, with values like 0.02 sec/ft^2 within the wake at 150 kft. Corresponding diffusion distances for flight at 2 x 10^4 fps and $\delta_c = 1$ ft are about 4 x 10^3 ft. Reduced temperatures T due to chemical freeze decrease the values of $\mu/\rho \sim T^{-3/2}$, thereby increasing the diffusion times. A profile aberation with typical dimension $\delta_c/3$ damps in a distance about 9 times shorter than the main flow.

In contrast to laminar cores, turbulent cores (Refs. 18-21) possess transports which dominate those of the shock induced vortical region, transports in the latter being essentially negligible. Only mean values are of concern here, and questions of stability, transition, persistence of turbulence, and edge-intermittency of turbulent free-mixing are not considered.

A turbulent core grows essentially in the well-known manner of turbulent free-mixing (Ref. 24) subject to some average "inviscid" outer values of the shock induced regime. Additional refinement is achieved by taking into account the local changes in outer edge conditions of the core as the core progressively entrains the vortical outer mass. In both the laminar and turbulent mixing regions true similarity is achieved only after substantial decay to uniformity has taken place. Prior to the region of similarity the lateral growth of high temperature mixing regions is inhibited by the heat sink effect of cooler outer-flow.

Turbulent diffusion lengths are on the order of $\delta^2 \rho_r u_e/\mu_{t_o}$ where δ is the thickness of the region, say, the core radius, ρ_r is a reference density, μ_t is a turbulent "viscosity," u_e is a local velocity at the edge of the turbulent layer, and subscript o denotes evaluation at the axis. Based on an empirical constant-property relation, Bloom and Steiger (Ref. 22) have assumed that in compressible flow $\mu_{to} = \rho_r K(2\delta_m)(u_e - u_o)$, where $K \sim 0.01$, $\delta_m^2 = \int_0^\delta (\rho/\rho_r)\, y\, dy$, and y is the radial coordinate. This yields a length on the order of $\delta/2K(1-\bar{u}_o) \sim 100\delta$. An assumed value of $K \sim 0.001$ gives a length of 1000 ; the latter values are comparable to those of the more detailed calculations to be shown here. This guess as to the nature of the turbulent transport indicates a length essentially independent of altitude for a given initial core width and velocity defect. Only experiments can yield a more reliable model. However, on this basis, laminar lengths at sufficiently high altitudes can be as short as turbulent ones, provided the turbulent wakes exist. For short wakes, one can envisage the possibility that simultaneous pressure gradient and diffusion effects will be of interest.

Quantitative estimates of wake properties are presented here within the framework of the boundary layer approximations and uniform pressure. Because of the nonsimilarity of the wake decay, integral methods (Refs. 22 and 23) are employed; other alternatives require linearization, assumption of local similarity, or finite-difference calculations. The integral method (Ref. 22) involves satisfying the conservation equation both on the average and exactly along the central axis, by means of an appropriate number of arbitrary parameters permitted to remain free in assumed profiles.

Specifically, in the present solution which follows Ref. 22, a density transformation of the radial coordinate is introduced, and polynomial profiles of parameters like $(u - u_e)/(u_o - u_e)$ are assumed. The momentum equation is satisfied both in integral form and on the axis. In the energy and species conservation equations the diffusion velocities are expressed by Fick's law as an approximation, the same diffusion coefficient D being assumed for each species. Thus an average constant Lewis number ($Le = \rho D c_p/k$, where c_p and k are the specific heat and conductivity of the mixture) as well as a constant Prandtl number ($Pr = \mu c_p/k$) is assumed for the mixture. In laminar flow Le and Pr are generally different from unity. In the turbulent flows treated here the turbulent counterparts of Le and Pr are each assumed equal to one.

To compromise between simplicity and accuracy, the energy and species conservation equations are satisfied along the axis, but the corresponding integral equations are ignored. This choice permits the representation of significant effects of Le and Pr in the important central region of the wake; these are averaged out in the integral equations.

When the flow is chemically frozen, the following relation between species concentration a_{io} and velocities $\bar{u}_o = u_o/u_e$ along the axis can be derived from the cited system; it indicates the effect of considering Le and Pr $\neq 1$

$$(a_{ie} - a_{io})/(a_{ie} - a_{ioc}) = \left[(1-\bar{u}_o)/(1-\bar{u}_{oc})\right]^{Le_o/Pr_o} \qquad (10)$$

Clearly the assumption $Le_o/Pr_o = 1$ leads to underestimates of the dispersion of species. For a ratio of velocity defect to the initial defect $(1-\bar{u}_o)/(1-\bar{u}_{oc}) = 0.5$, the value $Le_o/Pr_o = 2$ yields a mass fraction ratio of 0.25. Local temperatures are sensitive to this influence, due to their dependence upon small differences between the enthalpy h and the dissociation energies.

Also of interest is the effect of nonunity Pr_o and Le_o on the relation between stagnation enthalpy $\bar{H} = H/H_e$ and velocity $\bar{u} = u/u_e$. For Pr = Le = 1, the Crocco integral holds. Otherwise, one can write approximately along the axis

$$\frac{1-\bar{H}_o}{1-\bar{u}_{oc}} = \left(\frac{1-\bar{u}_o}{1-\bar{u}_{oc}}\right)\left[\frac{1-\bar{H}_{oc}}{1-\bar{u}_{oc}} + B \ln\left(\frac{1-\bar{u}_{oc}}{1-\bar{u}_o}\right)\right] \qquad (11)$$

where $B \sim (1-Pr_o)/Pr_o$. This reduces to the Crocco relation when B = 0.

Fig. 15a shows plots of Eq. 11 for uniform (dashed) and non-uniform (solid) initial stagnation enthalpy and for B = 0 and 0.3. When $\bar{H}$ is initially uniform, the effect of $Pr_o \neq 1$ is to diminish $\bar{H}_o$ about 5% and then to return it asymptotically to unity. This is the same trend as that observed in the equilibrium case. When $\bar{H}$ is not uniform initially, $\bar{H}_o$ moves monotonically to unity when B = 0, but has a minimum prior to its approach to unity downstream. These effects have their physical basis in the balance of phenomena signified by the Prandtl number.

Laminar wake calculations

Initial and flight conditions for a particular set of laminar

wake calculations (Ref. 22) are given in Table 2.

The initial wake radii are about 0.75 ft and the initial velocity ratios $\bar{u}_{oc}$ about 0.65. Altitudes are 150,200 and 250 kiloft and velocities about 2×10^4 fps. Uniform initial stagnation enthalpies $\bar{H}$ are assumed, save for one calculation for which $\bar{H}_{oc} = 0.9$.

In these calculations the initial conditions at the axis have been estimated by assuming the gas frozen at equilibrium state behind a normal shock and expanded isentropically to ambient pressure. The initial mass fractions of NO^+ and e^- thus obtained are somewhat high, since the process governing these species is actually in nonequilibrium, being faster than those of the other species, which are indeed frozen in the supersonic regime at altitudes above 150,000 ft. Actual relaxation conditions behind inclined portions of the bow shock have been considered in the third section.

The reaction rates for all species except NO^+ and e^- are sufficiently small here to be negligible in comparison with diffusion in the wake. For NO^+ and e^-, diffusion and chemical rates are considered simultaneously. The electron concentrations, shown in Fig. 14, are truly in nonequilibrium at the specified flight conditions. The corresponding equilibrium values at 150,000 ft are approximately 10^{-3} times those shown. Larger deviations from equilibrium occur at the higher altitudes. The nonunity values of Le and Pr, which lead to significant increases in temperature (Fig. 16) due to the aforementioned diffusion effect, have only a minor effect on the electron densities due to compensating decreases in density. The effects in lowering the stagnation enthalpies are shown in Fig. 15b.

Turbulent core calculation

The growth of a typical fully turbulent core within a vortical outer flow is calculated by the integral method on the basis of an assumed turbulent viscosity μ_t which must be subject to experimental evidence. As stated at the beginning of this section, the assumed expression is based on an empirical constant-property relation (Ref. 24) which is adapted to compressible flow as suggested in Ref. 22. The integral method requires its evaluation along the axis only, namely

$$\mu_{to} = K\rho_r(2\delta_m)(u_e - u_o) \qquad (12)$$

where subscripts o and e denote the axis and edge of the core, δ_m is the density transformed local core radius, ρ_r is a reference density, K is a pure constant on the order of 0.01 on

the basis of incompressible data, and all quantities except K may vary with x .

The integral method employed here is analogous to that described previously for laminar flow. For the illustrative conditions selected, a frozen composition of N_2, N, O_2, and O in both the core and vortical flow may be considered. The non-equilibrium electron trace-reaction is not treated. Uniform stagnation enthalpy and pressure are assumed.

The inviscid velocity profile u_e/u_∞ is correlated in terms of a mass-flow parameter η defined as

$$\rho_\infty u_\infty \eta^2/2 = \int_0^y \rho_e u_e \, y dy$$

where subscript e denotes conditions in the vortical flow and ∞ denotes undisturbed free stream conditions. Thus η signifies the frontal radius which contains a free stream mass-flow of the indicated magnitude.

The species profiles are obtained by noting that a_O is essentially constant when a_N is non-uniform, whereas a_N is virtually zero when a_O starts to change. Therefore, if the sensible enthalpy ($\sim c_p T$) is neglected with respect to the dissociation energies, and if small perturbations of velocities are observed, that is $(u_\infty - u_e)/u_\infty << 1$, the constancy of stagnation enthalpy leads to the result

$$2(h_e - h_\infty) = u_\infty^2 - u_e^2 \rightarrow a_O h_{dO} + a_N h_{dN} \cong u_\infty (u_\infty - u_e) \qquad (13)$$

where h is enthalpy and h_d is dissociation energy of indicated species.

On this basis, the inviscid species may be described as

$$0 < \eta \leq r_n : \quad a_O = 0.232, \quad da_N/du_e = -u_\infty/h_{dN}$$

$$1 < \eta < 1.5 r_n : \quad a_N << 1, \quad da_O/du_e = -u_\infty/h_{dO}$$

Within the core, which is diffusion dominated in this example, the turbulent Prandtl number and Lewis numbers are assumed equal to unity. As a result a Crocco integral relation may be derived for the stagnation enthalpy; that is, $H = A + Bu$, where A and B are constants. Consistency with external and initial conditions permits use of this relation only when H is constant.

The governing integral equations are the following:

Momentum:

$$\frac{d}{dx}\int_0^\delta \rho u(u_e - u)\,ydy - \left(\frac{du_e}{dx}\right)\int_0^\delta \rho u\,ydy = 0 \qquad (14)$$

Species conservation:

$$\frac{d}{dx}\int_0^\delta \rho u(a_{ie} - a_i)\,ydy - \left(\frac{da_{ie}}{dx}\right)\int_0^\delta \rho u\,ydy = 0 \qquad (15)$$

Introduction of Eq. 13 and the assumption

$$\frac{a_{ie} - a_i}{a_{ie} - a_{io}} = \frac{u_e - u}{u_e - u_o} \qquad (16)$$

produces the following equation for $a_{io}\ (x)$

$$\left[\frac{a_{ie} - a_{io}}{u_e - u_o} - B_i\right]\int_0^\delta \rho u(u_e - u)\,ydy = \text{constant} \qquad (17)$$

where the integration constant is evaluated at an initial station and the velocity field is obtained by steps analogous to those used in the laminar analysis (see Ref. 1).

The solution may be carried out in terms of a transformed streamwise coordinate s without prior specification of the group of empirical parameters $K\rho_r/\rho_c$, where ρ_c appears in the density transformation. For the present example a mean value is assigned to this group, namely $K\rho_r/\rho_c = 0.001$. The streamwise scale may simply be stretched in proportion to alternative mean values.

Conditions for the example are: altitude 200,000 ft; u_∞ = 23,000 fps, initial u_e = 14,000 fps, initial u_o = 8,200 fps, initial δ = 0.47 ft corresponding to an initial $\eta = 0.1$, $K\rho_r/\rho_c$ = 0.001. It is assumed arbitrarily that $\rho_c = \rho_\infty$.

The calculated results are presented in Fig. 17. The velocity decrement $(u_e - u_o)/u_e$ decays rapidly from 0.4 to 0.1 but then remains rather constant at about 0.1 as the edge velocity u_e approaches u_∞. Truly similar asymptotic behavior is not achieved until after the core has entrained the shock affected mass, that is, $\eta > 2.5\,r_n$, as evidenced by the core thickness δ. For $1 < \eta < 2$ (300 ft < x < 700 ft, where r_n = 1 ft and δ_c = 0.47 ft)

the core grows more strongly than the $x^{1/3}$ law. This trend is in rough agreement with those shown by core thicknesses measured in pellet firings (Refs. 18 and 21) at velocities between 5000 and 10,000 fps which show initial growths like $x^{1/2}$ or $x^{2/3}$ and then rapid change to the $x^{1/3}$ law. Initially, for $\eta < 0.5$ ($x < 100$ ft) the growth law is roughly similar, like $x^{1/3}$, since the edge velocity u_e is not much altered, and the mass entrained is relatively small in this regime.

The temperatures are extremely sensitive to changes in composition or velocity since

$$T \sim H - (u^2/2) - a_O h_{dO} - a_N h_{dN}$$

The axis temperature T_o exhibits a rather sharp drop from 9600 to 3800 R within 30 ft, constancy for the next 100 ft and then a reheating to about 6500 R. This temperature is maintained between 250 and 500 ft and then drops off again to approach the ambient level. The reheating is associated with the dispersion of atomic species.

BOUNDARY LAYER EFFECTS OVER THE BODY

Concern next centers on flow field structure and chemical behavior rather than on skin friction and heat transfer. Impermeable, noncatalytic surfaces are considered unless otherwise noted. Under these circumstances, mass conservation considerations dictate that the normal concentration gradients be zero at the surface.

Deviations from equilibrium in the boundary layer may be associated with two effects: 1) Surface conditions, such as low surface temperatures, which extend their influence from the interior; and 2) nonequilibrium conditions in the external inviscid flow, which continue into the boundary layer from the outer edge.

Typical manifestations of the former effect are encountered in the boundary layer at the stagnation point on a re-entry body (e.g., a spherical nose 1 ft in diameter at velocities of about 20,000 fps and altitudes below 200 kft). This problem has been investigated by Fay and Riddell (Ref. 25), who distinguished and described various situations on the basis of a recombination rate[10] parameter C_1

[10]The present definition takes into account more recent recombination rate values (Ref. 14) and approximations contingent with hypersonic conditions.

$$C_1 \simeq 0.2 \left(\frac{\rho_\infty}{\rho_a} \times 10^3\right)^2 \left(\frac{1}{15\epsilon}\right)^{2.5} \left(\frac{5000°K}{T_s}\right)^{1.5} \left(\frac{2 \times 10^4 fps}{u_\infty}\right) \left(\frac{r_n}{1\ ft}\right)$$

where ρ_∞ is the density at altitude, ρ_a is the sea level density, ϵ is the ratio of free-stream to post-shock density, T_s is the stagnation temperature in deg K, u_∞ is the flight velocity, and r_n is the nose radius in ft. Values of $C_1 > 10^{-1}$ denote equilibrium conditions, whereas $C_1 \leq 10^{-5}$ indicates complete freeze of atom concentrations; clearly the departure from equilibrium is encountered abruptly as the altitude is increased. Additional work by Grier and Sands (Ref. 26) indicates that both increased wall temperatures and decreased velocities lead to moderate decreases in the altitudes required for freeze.

The second effect listed in the introduction to this section becomes readily apparent as the boundary layer flow around the body is considered. In cases where equilibrium prevails at the stagnation point in presence of a cold wall, departures from equilibrium arise first in the inviscid flow and in outer portions of the viscous layer.[11] The station on the body where these departures are manifested first can readily be estimated by considering the ratio between the local value of the rate parameter and that at the stagnation point, namely

$$\frac{C_1}{(C_1)_s} = \left(\frac{p}{p_s}\right)^2 \left(\frac{T}{T_s}\right)^{-2} \frac{(du_e/dx)}{u_e/x} \tag{18}$$

Subsequently the freeze penetrates into the boundary layer from the outer edge, while the inner portion of the layer remains in nonequilibrium, but unfrozen. As one proceeds around the body penetration of freeze extends to distances arbitrarily close to the surface. Sufficiently far downstream (on a blunt nosed slender body with noncatalytic wall), the boundary layer becomes essentially frozen; however, the species profiles are not uniform because of the prior history. There follows an asymptotic decay to uniformity in the streamwise direction; the latter process is analogous to that which occurs when a heat source or sink is located upstream of an adiabatic surface, and the surface temperature along the wall adjusts to the adiabatic value. In view of this behavior it becomes of interest to estimate where and if the freeze can (practically) reach the wall on a given configuration. Approximate information in

[11] If nonequilibrium prevails at the stagnation point only the subsequent considerations relative to the asymptotic behavior of the boundary layer are of interest.

this connection can be reasoned out from an integral method approach as presented by Chung and Anderson (Ref. 27), who describe the species concentrations in a nonequilibrium situation by profiles like

$$m_i\left(\frac{x}{L_B}, N\right) = \Phi_i(m_{iw}, N) + \Gamma_i\left(\frac{x}{L_B}\right)\Omega_i(N) \tag{19}$$

where m_i is the ratio of mass fractions a_i/a_{ie}, x is the streamwise coordinate, L_B is a typical body dimension, N is the density transformed coordinate normal to the wall, and (denoting by Sc the Schmidt number)

$$\Gamma_i = -\frac{Sc}{a_e}\frac{x}{u_e}\left(\frac{W_i}{\rho}\right)_w O(10) = O(10)\left(\frac{T_e}{T_w}\right)^{3.5} C_1 \tag{20}$$

The function Φ_i is chosen to represent the frozen profile for a given value of m_{iw}, while the function Ω_i acts as a perturbation due to chemical reaction within the boundary layer. If Φ_i and Ω_i are expressed by fifth and sixth degree polynomials, respectively, the concentration profile takes the form

$$m_i = m_{iw} + (1-m_{iw})(10N^3 + 15N^4 + 6N^5) + \frac{\Gamma_i}{2}(N^2 - 4N^3 + 6N^4 - 4N^5 + N^6) \tag{21}$$

The quenching action of the wall is clearly exhibited by inspection of the leading terms for small N, namely $10N^3$ and $\Gamma_i N^2$. The latter always dominates over a small region near the wall, which, however, becomes negligible (say $N \leq 10^{-2}$) if $\Gamma_i \leq 1/10$; for lower values of Γ_i the behavior of a fully frozen boundary layer over a non-catalytic wall is approached. An estimate of the asymptotic approach to uniformity can be made by postulating similarity of the function $(a_i - a_{ie})/(a_{iw} - a_{ie}) = g(N)$ in the species conservation relation for frozen flow. Here a_{iw} is a function of x, a_{ie} is constant. The transformed conservation relation takes the form

$$\left(\frac{Le}{Pr}\frac{\rho\mu}{\rho_e\mu_e}g'\right)' + Fg' - 2\phi F'g = 0$$

where $F(N)$ is the Blasius function, primes denote differentiation with respect to N, $u/u_e = F(N)$, ϕ is a constant defined by

$$\phi = [s/(a_{iw} - a_{ie})][d(a_{iw} - a_{ie})/ds]$$

and

$$s = \int_0^x \rho_e \mu_e u_e y_b^{2j} \, dx$$

Thus

$$a_{iw} - a_{ie} \sim s^{\phi}$$

Now an integral equation formed from the species conservation relation, taking into account the zero concentration gradient condition of the noncatalytic wall and the required similarity yields the decay law

$$a_{iw} - a_{ie} \sim s^{-1/2} \tag{22}$$

In the special cases of uniform inviscid flow (wedges or conical bodies), the simple relations $s \sim x^{2j+1}$ and $a_{iw} - a_{ie} \sim x^{-(j+1/2)}$ are obtained.

There appears to be little advantage to further idealization of boundary layer calculations which involve partial regions of nonequilibrium or frozen flow; however, refined nonlinear studies of asymptotic nonequilibrium behaviors are clearly in order.

Viscous displacement effects in the shock layer

Viscous interaction gives rise to two important effects within the present context: 1) Increased pressures and densities in the viscous and inviscid flows strongly influence three-body recombination rates which are essentially proportional to ρ^2; commensurately density sensitive properties such as electron-densities are influenced; 2) the inviscid changes feed back and alter the extent of the boundary layer displacements, which, in turn, influence the profiles of parameters such as temperature and electron density. Displacement induced pressures for two-dimensional flows may be estimated from interaction theories as summarized and extended in Ref. 10, for example. Under high altitude conditions, pressure rises of as much as an order of magnitude may be antitipated on two-dimensional surfaces at small or moderate incidence. These tend to drive the flow toward chemical equilibrium. However, on three-dimensional bodies, the rises are reduced to factors less than 2 due to three-dimensional relief. Furthermore, if a rough estimate is made of their effect on local particle-isentropic densities, it is noted that

$$\rho/\rho_\infty \simeq (1/\epsilon)(p/p_s)^{1/\gamma}$$

and, therefore, that local densities are increased less strongly than the pressures. Inspection of Eq. 18 then indicates a very weak dependence of chemical effects upon viscous-inviscid interactions.

OTHER EFFECTS

Unsteadiness of wake flows

Unsteadiness may arise by virtue of time dependence of the conditions at the outer edge of the viscous layer (e.g., changes in the speed or altitude of the generating body), by time dependence of the initial conditions (e.g., initial momentum defect, which is proportional to the drag of the body and may vary with angle of attack), etc.

Effect of changes in speed are considered first. The flows may be considered as quasi-steady when the diffusion times $\delta^2\rho_o/\mu_o$ are small in comparison with characteristic times for the induction of unsteadiness, e.g.: $[u_e/d^n u_e/dt^n]^{1/n}$ where n indicates the order of the time derivative and t denotes time. In turbulent flows a characteristic turbulent viscosity μ_{to} replaces μ_o in the diffusion times; since $\mu_{to} >> \mu_o$ and $\delta_t < \delta_e$ criteria which exhibit quasi-steadiness for laminar flows will also do so for turbulent flow under the same conditions.

In missile flight, decelerations on the order of 100g may be encountered at velocities on the order of 20,000 fps. For more extreme trajectories decelerations of as much as 600g and velocities on the order of 40,000 fps may arise. The corresponding unsteadiness times are 7 and 2 sec, respectively. According to the prior discussion of laminar diffusion times $\rho_o/\mu_o \approx 0.20$ sec at 100,000 ft altitude. Therefore, for characteristic wake radii $\delta \sim 1$ ft., the ratio $[\delta^2\rho_o/\mu_o]/[u_e/(du_e/dt)] \leq 0.1$ and the flows can be considered as quasi-steady provided that the higher velocity derivatives are of the same order as the first. At lower altitudes the unsteadiness becomes more pronounced; however, the onset of turbulence must be taken into account.

Unsteady effects due to changes in density with altitude are also negligible for re-entry conditions. In fact, time differentiation of the model density-altitude variation: $\rho/\rho_o = e^{-\Lambda(z-z_o)}$ (where subscript o denotes a reference altitude) together with the approximation $dz/dt \sim u_e$, yield the characteristic density change time: $[\rho/(d\rho/dt)] = -1/\Lambda u_e \sim 1$ sec for $u_e \sim 2 \times 10^4$.

Variation in initial momentum defect due to oscillation of the generating body may be characterized by the period of the oscillations $1/\omega$. For quasi-steadiness to obtain with laminar flow is is, required that, for example

$$[\delta^2 \rho_o/\mu_o]\omega \simeq 0.02\omega << 1 \quad \text{at 150,000 ft}$$

Correspondingly ω is smaller than 5 cps. Thus, appreciable unsteady effects due to pitch oscillations may be encountered in practice.

Effects of heat loss by radiation in the stagnation region

For extremely high speed re-entry bodies, such as Mars probes, heat loss from the shock layer air due to radiation both to the cold body and to the outer atmosphere may have a noticeable effect on the state of the flow field.[12] To assist in the preliminary thinking about chemical effects of radiation losses, an extremely crude model is used here to derive some rough numerical values. It is postulated that an amount of heat characterized by a fraction $(1 - \epsilon)$ of the stagnation enthalpy is lost in the nose region at constant pressure.[13] The flow is then expanded isentropically to free stream pressure. Equilibrium conditions are assumed throughout. Typical resulting temperatures and electron densities are plotted in Fig. 18. As would be expected, the temperatures and electron densities are reduced by virtue of the heat loss. In view of the substantial effects on observables it will be of interest to perform

---

[12]This is not the case for re-entering missiles and satellites (Ref. 28).

[13]Consideration of the orders of heat loss per unit mass by radiation can be made on the basis of the following expression proposed by Lees (Ref. 29) (taking into account emissivity estimates of Kivel and Bailey (Ref. 30) among others) (Btu/ft^{2}sec) $\frac{q_{rad}}{r_n\,(ft)} \simeq 1.33 \left(\frac{\rho_\infty}{\rho_a}\right)^{1.3} (u_\infty \times 10^{-4}\ \text{fps})$. Values of ϵ in the range postulated for the calculations just given are justified thereby. With the approximate nose surface area $2\pi r_n^2$ and frontal mass flow $\rho_\infty u_\infty \pi r_n^2$, and with T_{av} the average nose layer temperature, this yields

$$1 - \epsilon = \left(\frac{T_{av}}{T_s}\right)^{12.5} 1.75 \times 10^{-6} \left(\frac{\rho_\infty}{\rho_a}\right)^{0.3} (u_\infty \times 10^{-4}\,\text{fps})^{9.5}$$

more accurate investigations.

CONCLUSIONS

Hypersonic flows about blunt nosed slender bodies have been investigated with emphasis on the aerothermochemical aspects of the problem. Attention has been directed toward a broad delineation of observables for flight regimes wherein distinct discontinuity (shock) surfaces and separate regions of inviscid and viscous flow can be recognized.

Study of the inviscid flow has shown that use of a simplified model in combination with one-dimensional rate calculations along streamlines can lead to reasonably accurate description of the actual situation. In fact, the rate calculations suggest and substantiate the model. The analysis has also provided interesting information on the purely fluidynamic aspect of the problem to the effect that similitude of flows about blunted plates and cylinder applies strictly only at very large distances from the nose ($\sim$ 1000 nose radii). In regions of practical interest, closer to the nose, the thickness of the entropy layer cannot be neglected. Here the flow must be studied by a model involving two layers; the inner layer is characterized by constant pressure and the outer layer by a self-similar small perturbation solution with a similarity parameter dependent upon nose shape and gas behavior. Recognition of this situation has led to a formal solution of the problem, to an accompanying correlation of a large number of data, and to the establishment of relatively simple rules for carrying out estimates.

Analysis of regions of viscous flows has emphasized wakes both laminar and turbulent. Numerical results have been reported for both situations; though a semiempirical approach was adopted in the turbulent case, computed wake thicknesses reproduce the trends observed in recent firings. Here the interesting feature is provided by the very rapid diffusion in presence of turbulence and by the related strong influence on observables.

The classical question of stability is still open; this as well as problems involving nonequilibrium boundary layers, additional physico-chemical effects (such as radiation), more complicated fluidynamic situations (such as three-dimensional flows), are in need of further investigation before the quantitative evaluation of external hypersonic flows including chemical reactions can attain a definitive standard.

ACKNOWLEDGMENT

The authors with to express their appreciation to the General Applied Science Laboratories, Inc. for permission to use machine programs and some technical material. Also, they wish to acknowledge the cooperation of M. Trella and M. H. Steiger in various phases of the investigation.

REFERENCES

1 Vaglio-Laurin, R. and Bloom, M.H., "Chemical Effects in External Hypersonic Flows," ARS preprint 1976-61; also Polytechnic Institute of Brooklyn, PIBAL Rep. no. 640, AFOSR 1273, Aug. 1961.

2 Freeman, N.C.: "Nonequilibrium Flow of an Ideal Dissociating Gas," J. Fluid Mech., vol. 4, pt. 4, Aug. 1958, pp. 407-425.

3 Freeman, N.C.:, "On a Singular Point in the Newtonian Theory of Hypersonic Flow," J. Fluid Mech., vol. 8, pt. 1, May 1960, pp. 109-122.

4 Lick, W., "Inviscid Flow of a Reacting Mixture of Gases Around a Blunt Body," J. Fluid Mech., vol. 7, pt. 1, Jan. 1960, pp. 128-144.

5 Cheng, H.K., "Similitude of Hypersonic Real-Gas Flows over Slender Bodies with Blunted Noses," J. Aero Space Sci., vol. 26, no. 9, Sept. 1959, pp. 575-585.

6 Feldman, S., "Numerical Comparison Between Exact and Approximate Theories of Hypersonic Inviscid Flow Past Slender Blunt-Nosed Bodies," ARS J., vol. 30, no. 5, May 1960, pp. 463-468.

7 Vaglio-Laurin, R. and Trella, M., "A Study of Flow Fields about Some Typical Blunt-Nosed Slender Bodies," Aero Space Eng., vol. 20, no. 8, Aug. 1961, p. 20.

8 Sychev, V.V., "On the Theory of Hypersonic Gas Flow with a Power-Law Shock Wave," J. Appl. Math. and Mech., vol. 24, no. 3, 1960, pp. 756-764.

9 Kochina, N.N. and Mel'nikova, N.S., "Strong Point-Blasts in a Compressible Medium," J. Appl. Math. and Mech., vol. 22, no. 1, 1958, pp. 1-19.

10 Cheng, H.K., Hall, G.J., Golian, T.C., and Hertzberg, A., "Boundary Layer Displacement and Leading-Edge Bluntness Effects in High Temperature Hypersonic Flow," J. Aero Space Sci., vol. 28, no. 5, May 1961, pp. 353-381.

11 Whalen, R.J., "Viscous and Inviscid Nonequilibrium Gas Flows," IAS Paper no. 61-23.

12 Van Hise, V., "Analytic Study of Induced Pressure on Long Bodies of Revolution with Varying Nose Bluntness at Hypersonic Speeds," NASA TR 78, 1961.

13 Gaitatzes, G. and Bloom, M.H., "On the Interior of Normal Shocks According to Continuum Theory, Including Rate Thermochemistry," Polytechnic Institute of Brooklyn, PIBAL Rep. no. 548, ARL 65, June 1961.

14 Wray, K., Teare, J.D., Kivel, B. and Hammerling, P., "Relaxation Processes and Reaction Rates Behind Shock Fronts in Air and Component Gases," Avco-Everett Research Lab., Research Rep. 83, Dec. 1959.

15 Bloom, M.H. and Steiger, M.H., "Inviscid Flow with Nonequilibrium Molecular Dissociation for Pressure Distributions Encountered in Hypersonic Flight," J. Aero Space Sci., vol. 27, no. 11, Nov. 1960, pp. 821-835.

16 Eschenroder, A.Q., Boyer, D.W. and Hall, G.J., "Exact Solutions for Nonequilibrium Expansions of Air with Coupled Chemical Reactions," Cornell Aeronautical Lab., Rep. no. AF-1413-A-1, May 1961.

17 Chapman, D.R., "An Analysis of Base Pressure at Supersonic Velocities and Comparison with Experiment," NACA Rep. 1051, 1951.

18 Dana, T.A. and Short, W.W., "Experimental Study of Hypersonic Turbulent Wakes," Convair, Physics Sec. ZPh-103, May 1961.

19 Demetriades, A., "Some Hot-Wire Anemometer Measurements in a Hypersonic Wake," 1961 Heat Transfer and Fluid Mech. Inst., Stanford University Press, 1961.

20 Lees, L. and Hromas, L., "Turbulent Diffusion in the Wake of a Blunt-Nosed Body at Hypersonic Speeds," Space Technology Labs., Aerodynamics Dept. Rep. no. 50, July 1961.

21 Slattery, R.E. and Clay, W.G., "Width of the Turbulent Trail Behind a Hypervelocity Sphere," Phys. Fluids, vol. 4, no. 10, Oct. 1961, pp. 1199-1201.

22 Bloom, M.H. and Steiger, M.H., "Hypersonic Axisymmetric Wakes Including Effects of Rate Chemistry," General Applied Sciences Labs. Rep. no. 180, Sept. 1960.

23 Feldman, S., "On Trails of Axisymmetric Hypersonic Blunt Bodies Flying Through the Atmosphere," J. Aero Space Sci., vol. 28, no. 6, June 1961, pp. 433-449.

24 Schlicting, H., "Boundary Layer Theory," McGraw-Hill Book Co., New York fourth ed., 1960, pp. 596-603.

25 Fay, J.A. and Riddell, F.R., "Theory of Stagnation Point Heat Transfer in Dissociated Air," J. Aero Space Sci., vol. 25, no. 2, Feb. 1958, pp. 73-85.

26 Grier, N.T. and Sands, N., "Regime of Frozen Boundary Layers in Stagnation Region of Blunt Re-entry Bodies," NASA TN D-865, May 1961.

27 Chung, P.M. and Anderson, A.D., "Heat Transfer Around Blunt Bodies with Nonequilibrium Boundary Layers," 1960 Heat Transfer and Fluid Mech. Inst., Stanford University Press, 1960.

28 Bird, G.A., "The Effect of Thermal Radiation on the Inviscid Hypersonic Flow Over a Blunt Body," J. Aero Space Sci., vol. 27, no. 9, Sept. 1960, p. 713.

29 Lees, L., "Heat Transfer at Hypersonic Speeds," in "Space Technology" (H. Seifert, ed.), John Wiley and Sons, Inc., New York, 1959.

30 Kivel, B. and Bailey, K., "Tables of Radiation from High Temperature Air," Avco Research Lab., Research Rep. 21, Dec. 1957.

31 Lin, S.C. and Teare, J.D., "A Streamtube Approximation for Calculation of Reaction Rates in the Inviscid Flow Field of Hypersonic Objects," Avco-Everett Research Note 223, Aug. 1961.

32 "Investigation of the Natural Interference Effects Upon High Thrust Piloted and Pilotless Vehicular Electronics System Performance," vol. 1, General Electric Co., Space Sciences Lab., WADD TR 61-191, Aug. 1961.

Table 1 List of cases computed

Case no.	Configuration[a]	Gas behavior[b]	Free stream conditions z (kiloft)[c]	Free stream velocity, U_∞ (fps)	Free stream Mach number, M_∞	Nose drag coefficients, C_D
1	a	frozen	298	26,050	28.20	.9
2	a	frozen	200	26,090	25	.9
3	a	equilibrium	200	26,090	25	.9
4	a	frozen	298	23,115	25	.9
5	a	frozen	200	22,960	22	.9
6	a	equilibrium	200	22,960	22	.9
7	a	equilibrium	150	23,070	21	.9
8	a	frozen	150	23.070	21	.9
9	b	frozen	298	23,115	25	.275
10	b	frozen	200	22,960	22	.275
11	b	equilibrium	200	22,960	22	.275
12	c	frozen	298	28,000	30.30	1.508
13	c	equilibrium	298	28,000	30.30	1.508

[a]See Fig. 2.
[b]Frozen denotes model behavior defined in the second section.
[c]Conditions defined by ARDC standard atmosphere at indicated altitude.
[d]Pressure drag coefficients referred to cross-sectional area of afterbody.

Table 2 Data for laminar wake calculations

Altitude (kiloft)		150	200	250
u_∞ (fps) x 10^{-3}		18.9	20.2	20.4
Conditions at altitude				
P_∞	(psf)	2.940	0.460	0.040
ρ_∞	(slugs/ft^3)	3.39×10^{-6}	5.88×10^{-7}	6.55×10^{-8}
T_∞	($^\circ$R)	504	454	354
μ_∞	(lb sec/ft^2)	3.58×10^{-7}	3.38×10^{-7}	2.71×10^{-7}
H_∞	(fps)^2	1.81×10^{8}	2.07×10^{8}	2.10×10^{8}
Initial conditions at axis				
α_O		0.232	0.232	0.232
α_N		0.133	0.213	0.245
(α_{NO^+}) x 10^3		0.563	0.566	0.485
n_e	particles/cc	4.44×10^{12}	8.13×10^{11}	6.89×10^{10}
ρ	(slugs/ft^3)	7.42×10^{-7}	1.35×10^{-7}	1.49×10^{-8}
$\bar{\rho} = \rho/\rho_\infty$		0.219	0.230	0.228
T	($^\circ$R)	1672	1352	1125
$\bar{H} = H/H_\infty$		1.0	1.0 0.9	1.0
$\bar{u} = u/u_\infty$		0.692	.656 0.574	0.634
δ_m	(ft)	0.5	0.5 0.5	0.5
θ_c	(ft^2) x 10^3	6.5	7.1 8.3	7.4
δ	(ft)	0.75	0.65	0.54

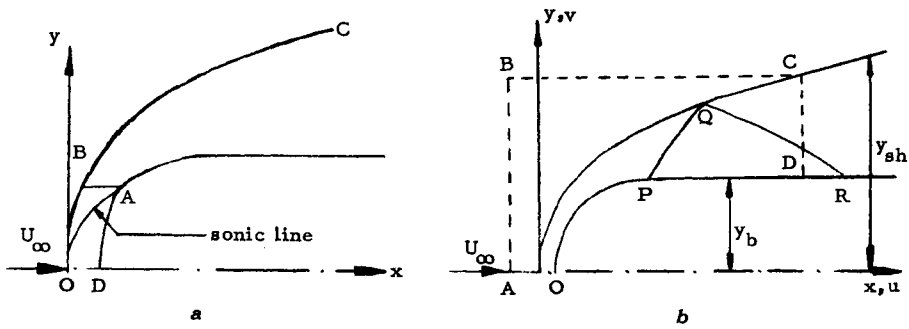

Fig. 1 Models for analyzing flow over blunt nosed bodies.

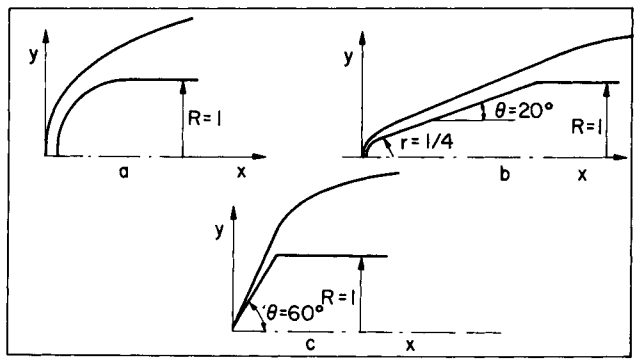

Fig. 2 Configurations analyzed in present report.

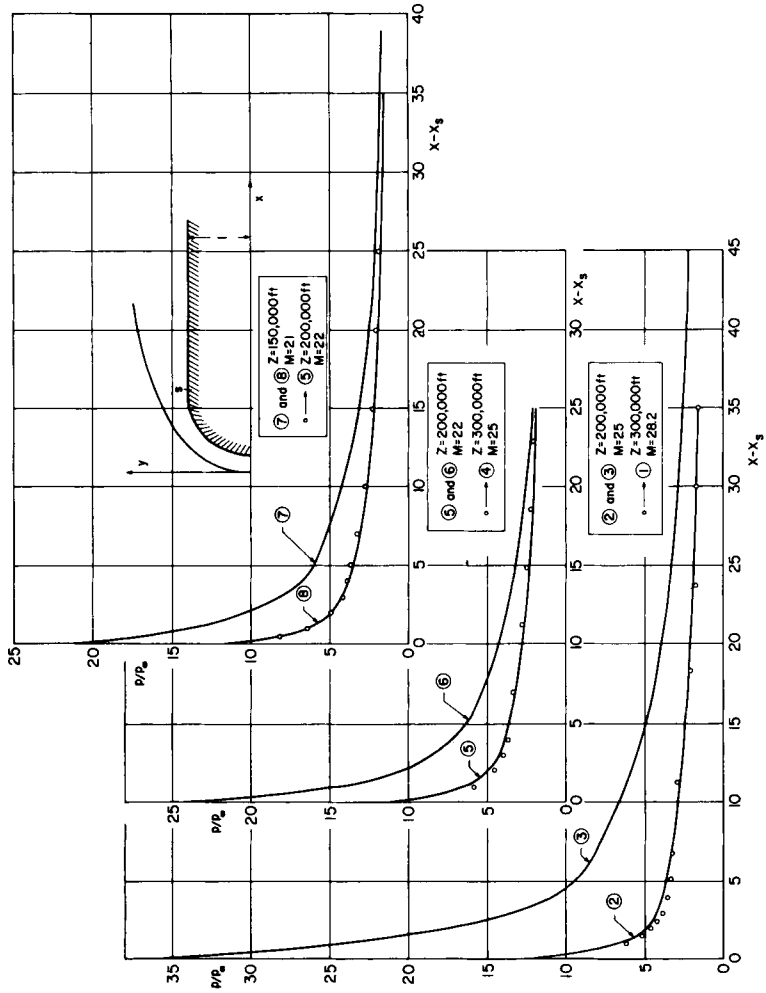

Fig. 3 Compilation of computed pressure distributions on cylindrical afterbodies for various flight conditions and either equilibrium or frozen gas behavior. Nose configuration a; cases 1,2,4,5,8 frozen; cases 3,6,7 equilibrium.

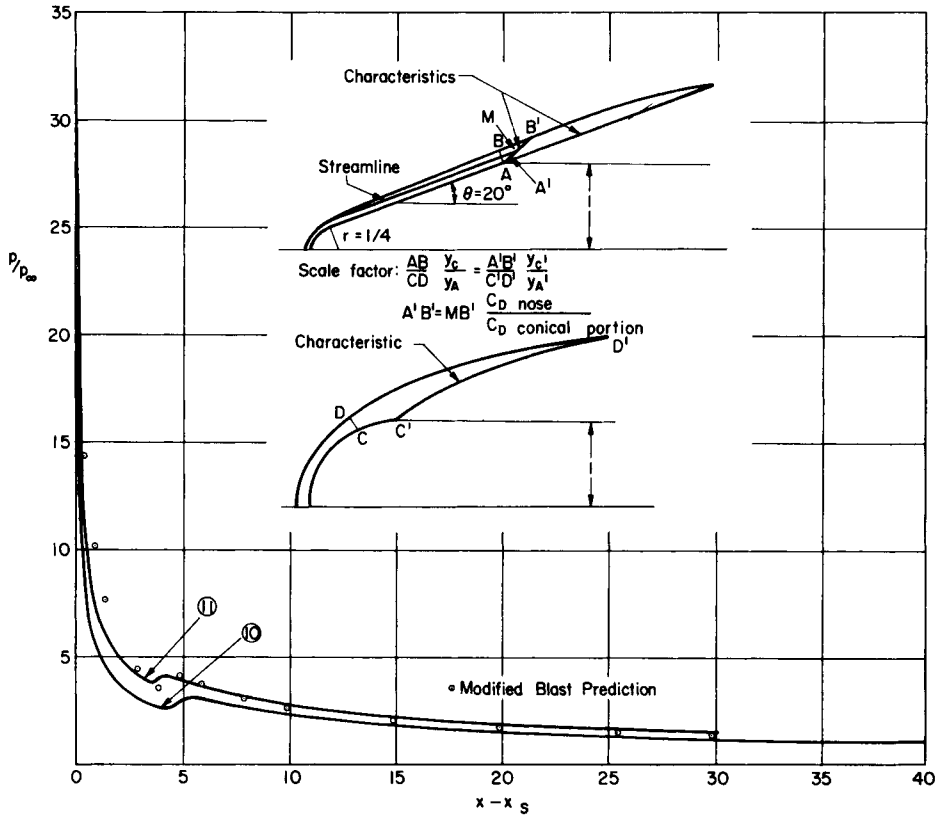

Fig. 4 Compilation of computed pressure distributions on cylindrical afterbodies for various flight conditions and either equilibrium or frozen gas behavior. Nose configuration b; case 10 frozen; case 11 equilibrium.

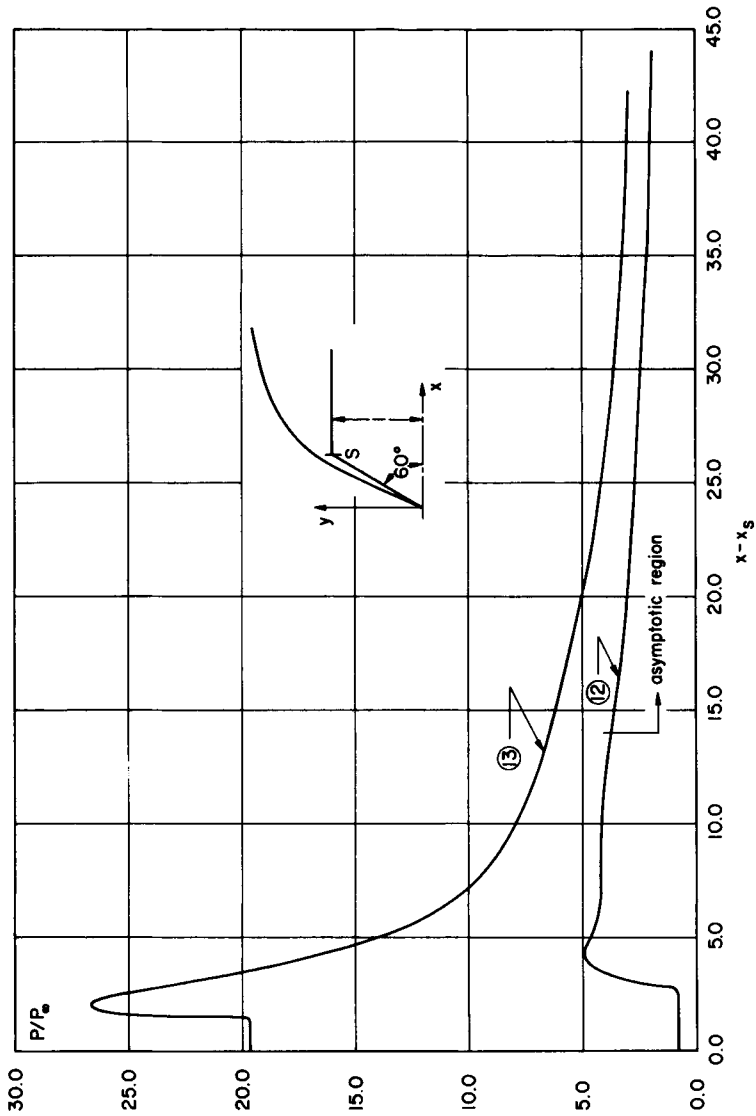

Fig. 5 Compilation of computed pressure distributions on cylindrical afterbodies for various flight conditions and either equilibrium or frozen gas behavior. Nose configuration c; case 12 frozen; case 13 equilibrium.

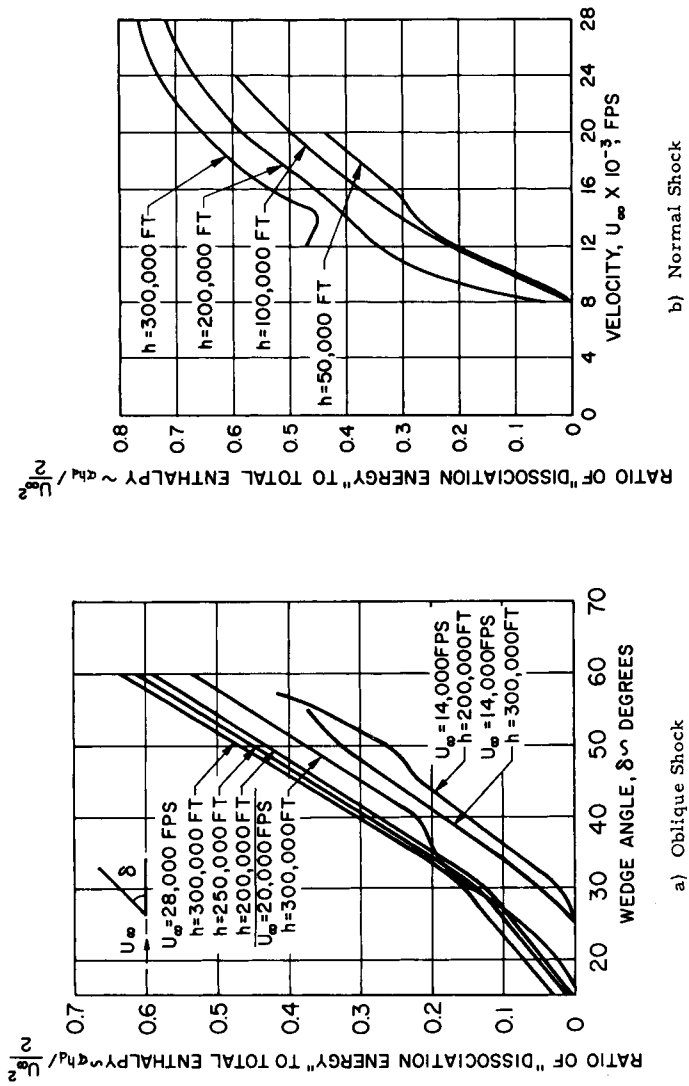

Fig. 6 Ratio of dissociation energy to free stream kinetic energy for equilibrium conditions behind a shock. Diagrams from Ref. 11.

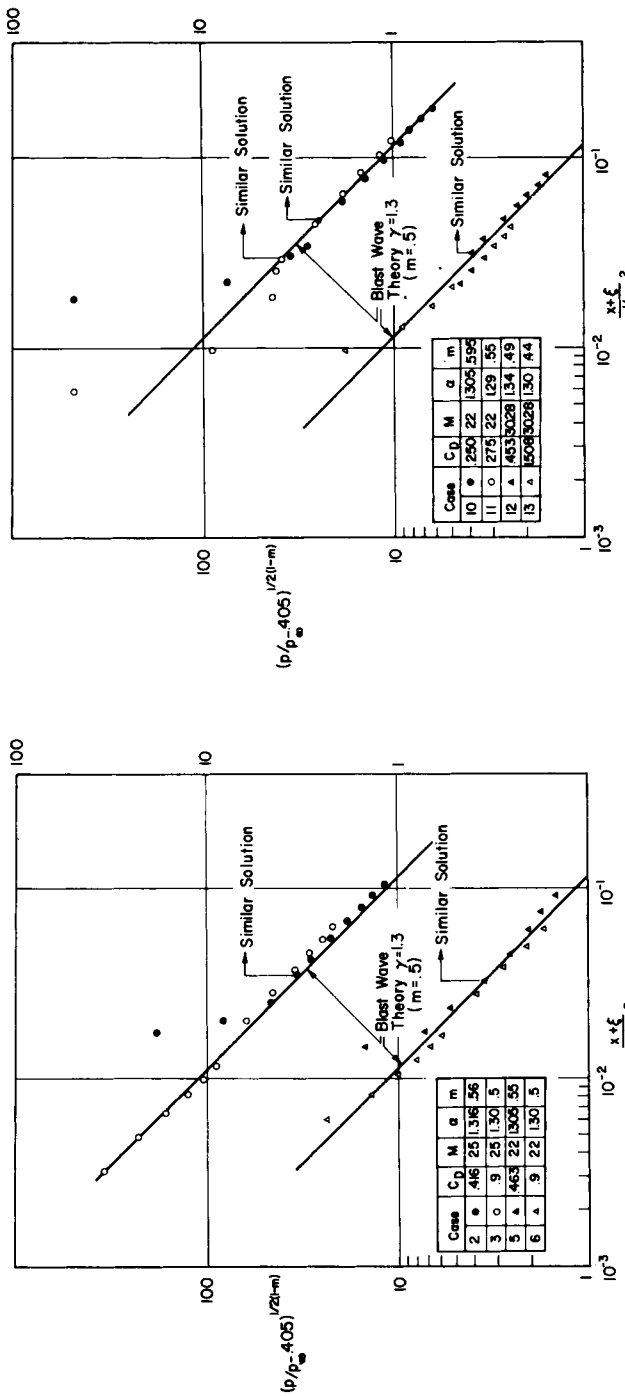

Fig. 7 Correlation of computed pressure distributions on cylindrical afterbodies for various configurations, flight conditions and gas behaviors.

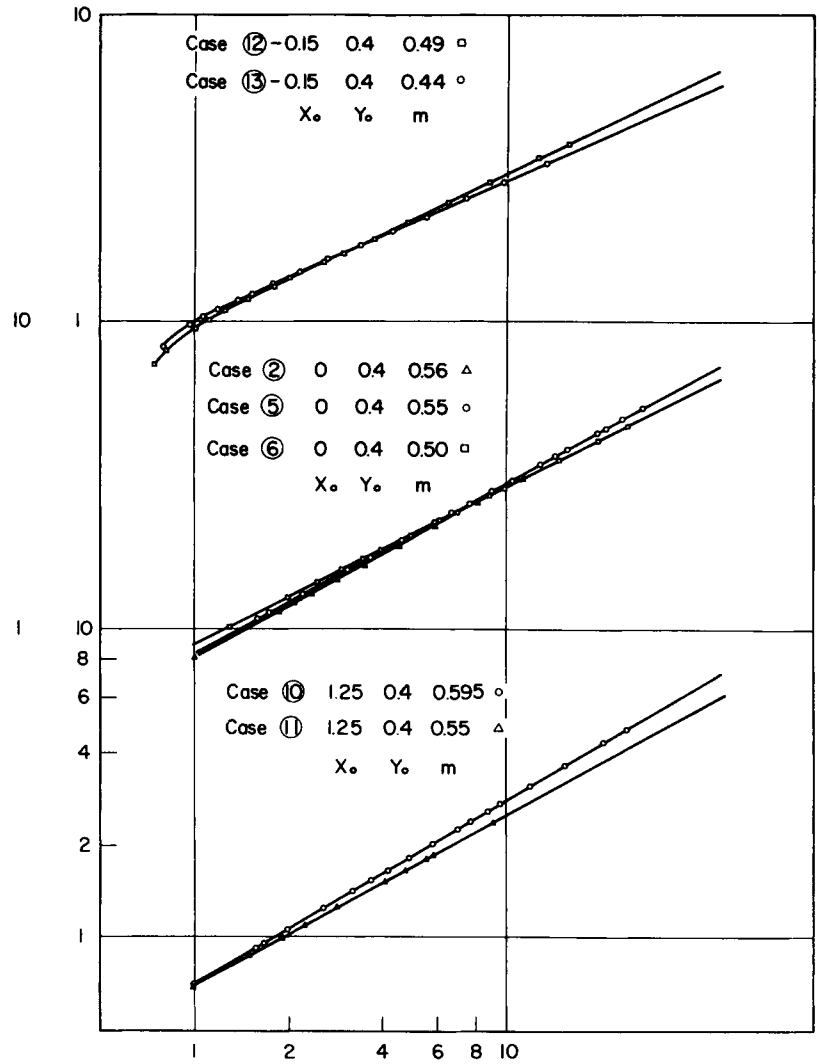

Fig. 8 Correlation of computed shock shapes for various configurations and gas behaviors. Top: Configuration c), $\bar{C}_{D_{12}} = .453$. Middle: Configuration a), $\bar{C}_{D_2} = .416$, $\bar{C}_{D_5} = .463$. Bottom: Configuration b), $\bar{C}_{D_{10}} = .250$.

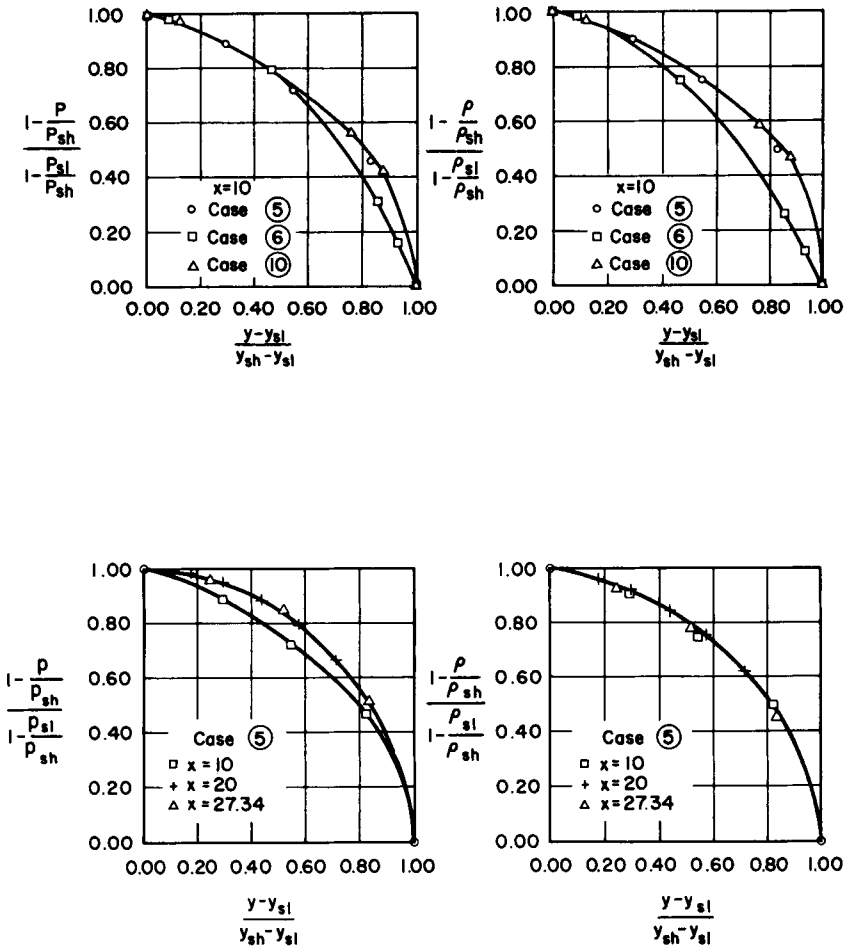

Fig. 9a Typical correlation of transverse distributions of pressure and density in the outer layer for various configurations and flight conditions. Top: Dependence upon shock exponent m . Bottom: Independence from axial coordinate.

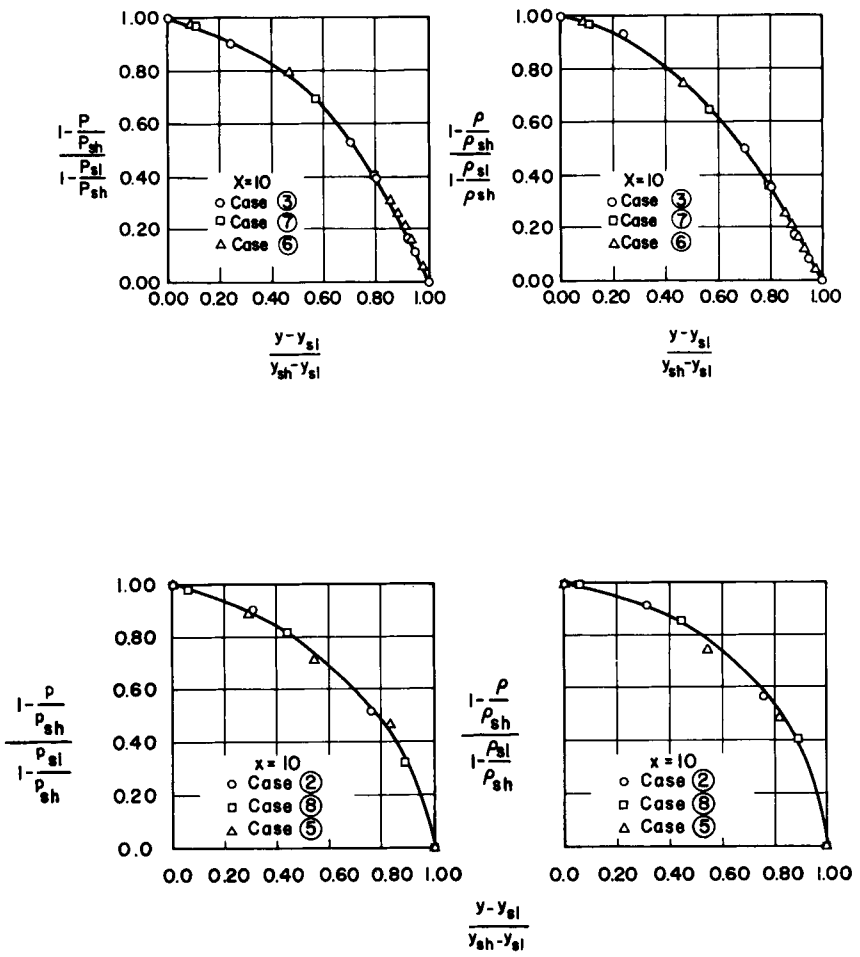

Fig. 9b Typical variation of transverse distributions of pressure and density in the outer layer for a given configuration, various flight conditions and gas behaviors. Top: Configuration a), equilibrium flow. Bottom: Configuration a), frozen flow.

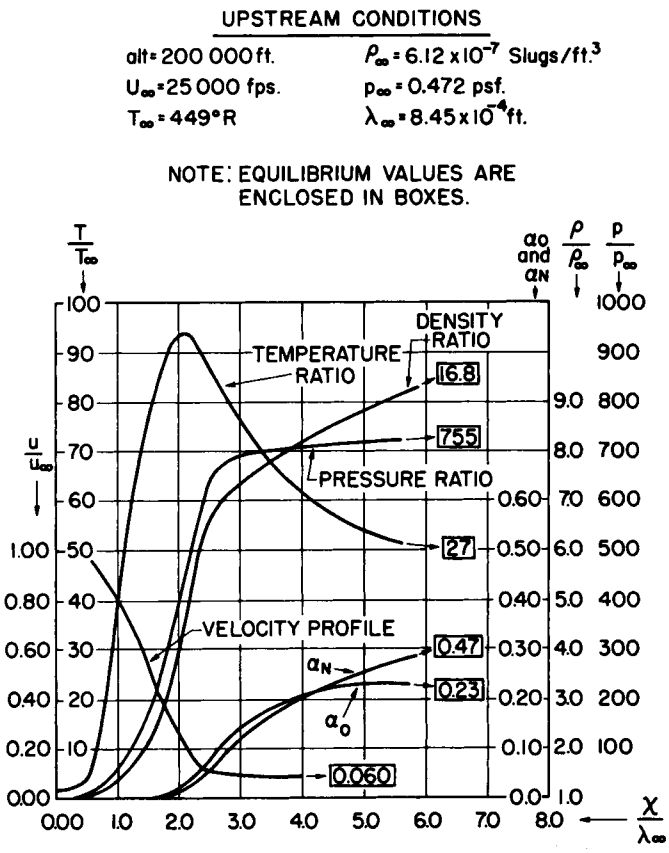

Fig. 10 Typical variation of flow properties across a normal shock wave in presence of rate dissociation. Mixture of oxygen and nitrogen partaking in reactions $N_2 \rightleftarrows 2N$, $O_2 \rightleftarrows 2O$. (x/λ_∞ denotes ratio of streamwise distance to mean free path in free stream; a_i denotes mass fraction of indicated species.)

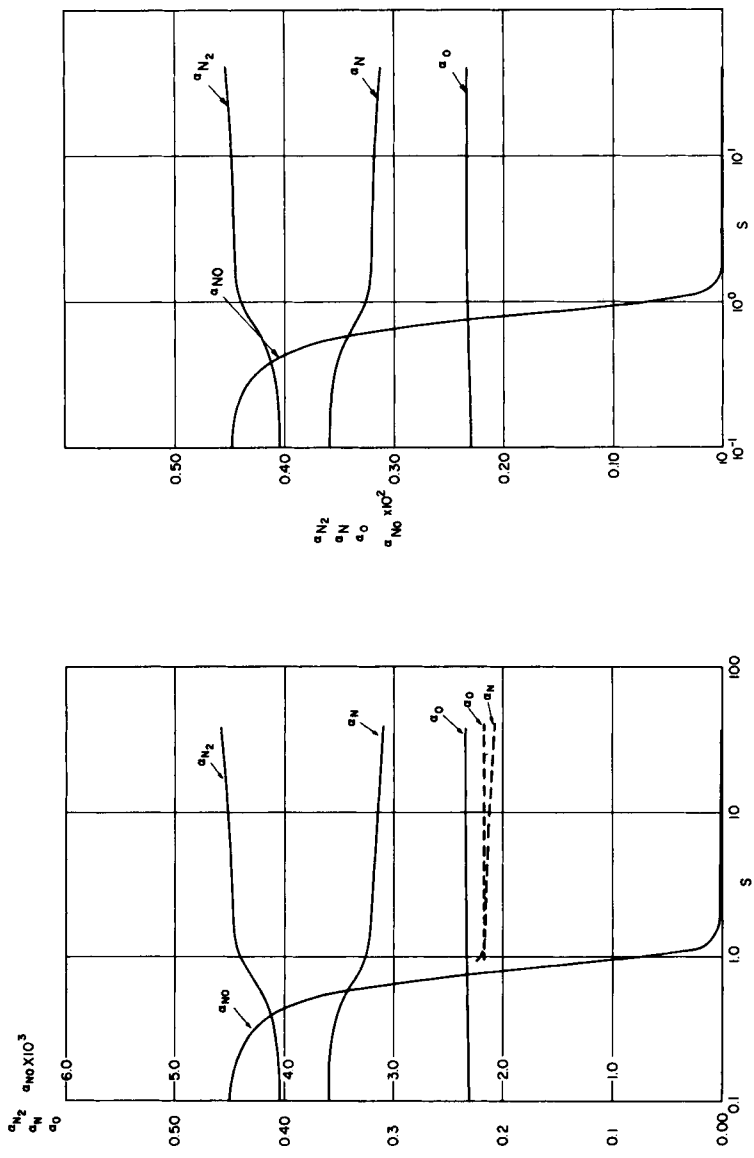

Fig. 11a Computed mass fractions of neutral species along a typical body streamline. Configuration a.). R = 1 ft, U_∞ = 23,000 fps. Left: Results obtained with pressure distribution for equilibrium flow z = 150,000 ft, --- z = 124,000 ft. Right: Results obtained with pressure distribution for frozen flow, --- z = 150,000 ft.

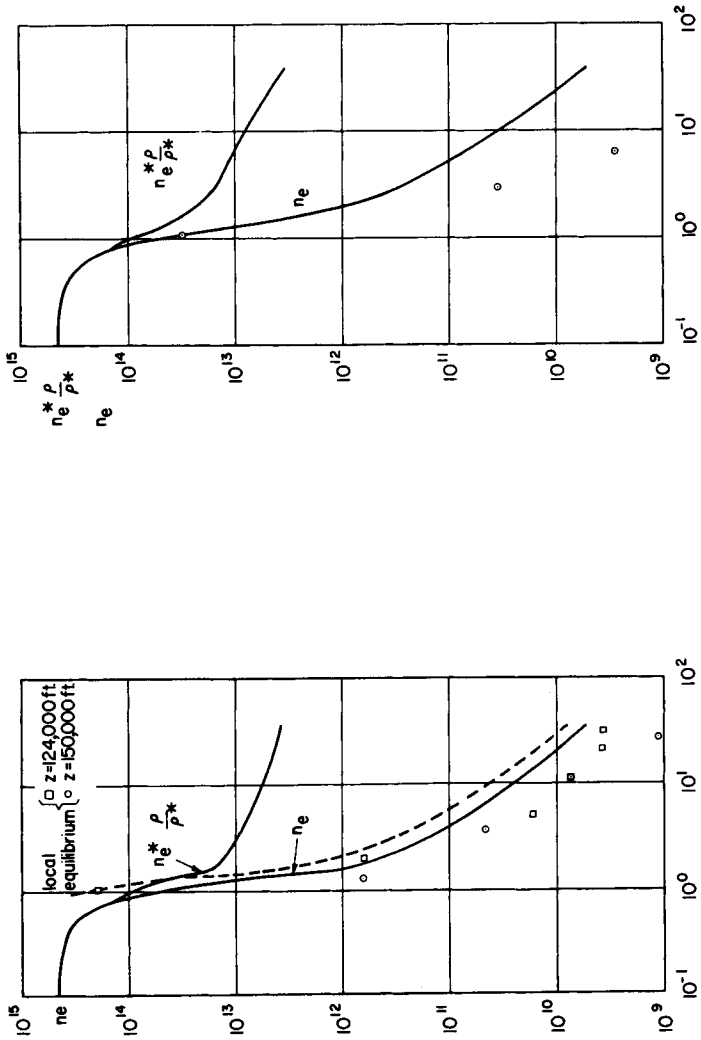

Fig. 11b Computed electron densities (particles/cc) along a typical body streamline. Configuration a), R = 1 ft, U_∞ = 23,000 fps. Left: Results obtained with pressure distribution for equilibrium flow, --- z = 150,000 ft, --- z = 124,000 ft. Right: Results obtained with pressure distribution for frozen flow, --- z = 150,000 ft.

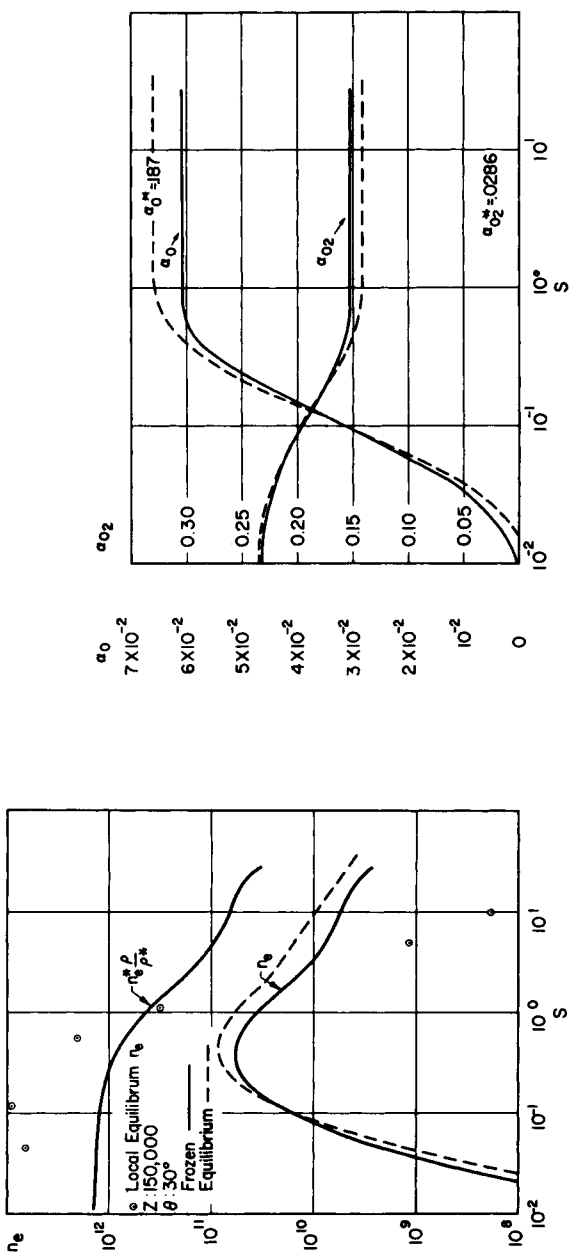

Fig. 12 Computed concentrations of various species along a streamline that intersects weak portion of the shock (deflection at shock = 30 deg. Configuration a), R = 1 ft, U_∞ = 23,000 fps, z = 150,000 ft, --- results obtained with pressure distribution for frozen flow; - - - results obtained with pressure distribution for equilibrium flow. Left: Electron densities (particles/cc). Right: Mass fractions of O_2 and O . *denotes equilibrium conditions behind given shock.

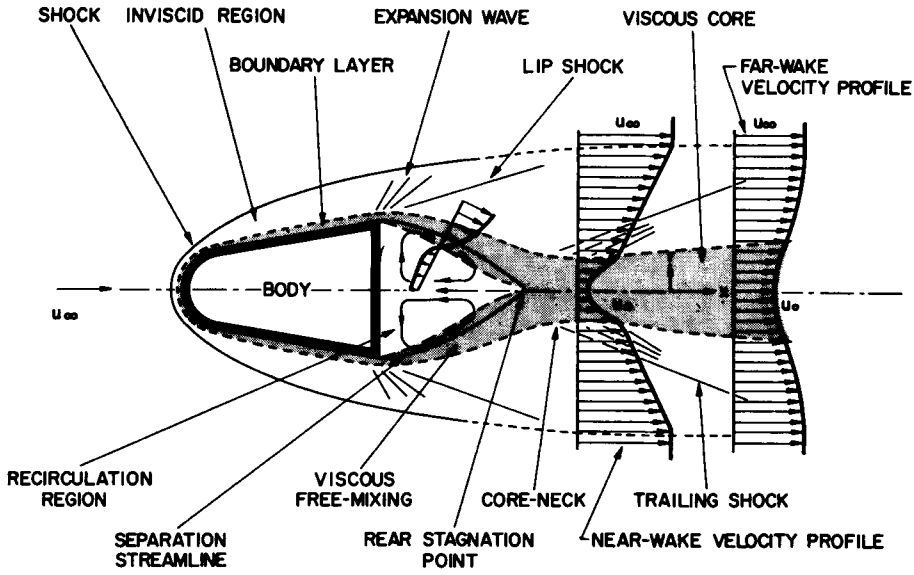

Fig. 13 Complete flow field around a blunt nosed body.

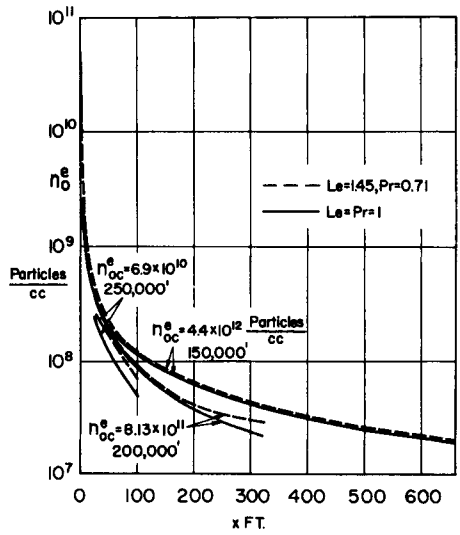

Fig. 14 Laminar wake: electron densities along axis ($\bar{H}_{oc}=1$).

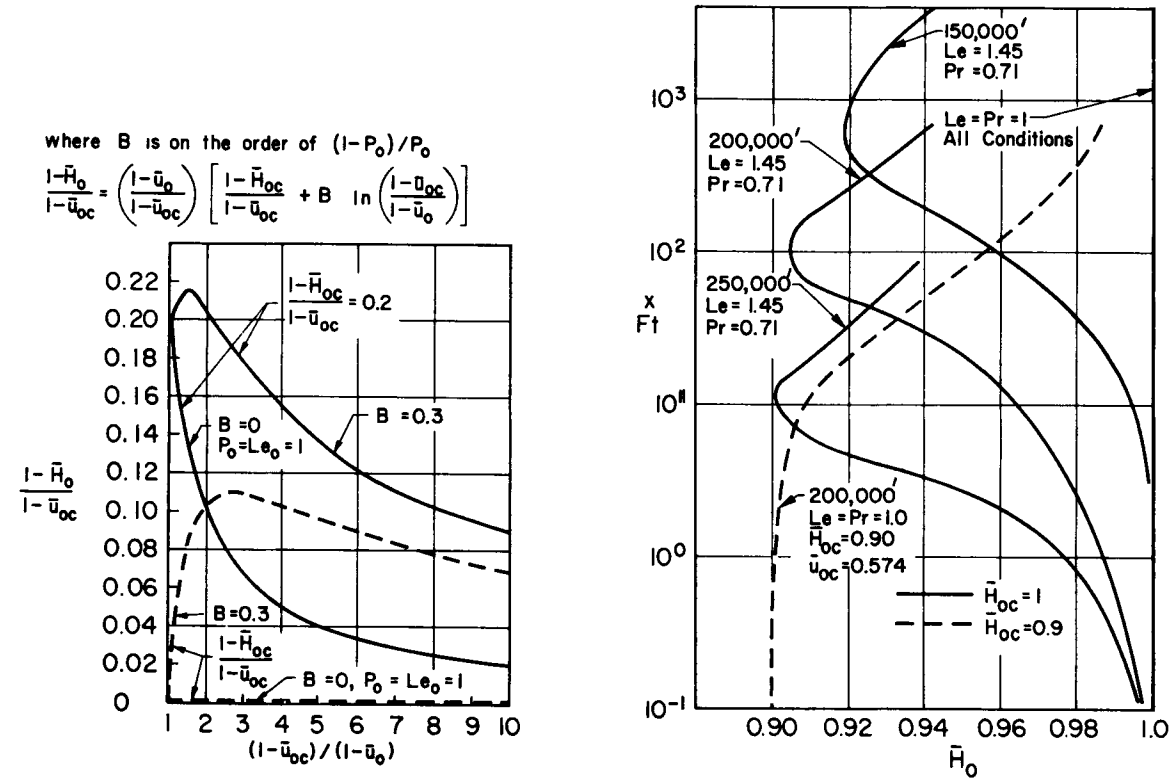

a. Estimated Effects of Non-unity Pr and Le

b. Results of Numerical Examples

Fig. 15 Laminar wake: stagnation enthalpy along axis.

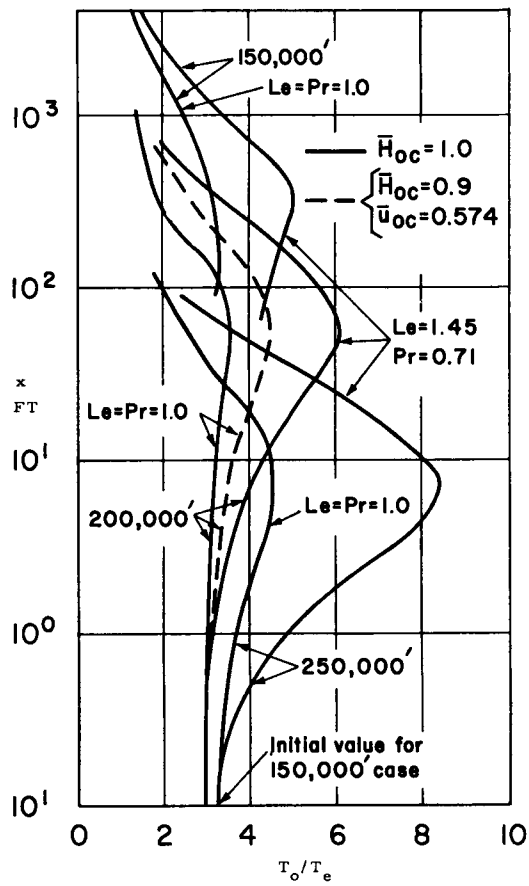

Fig. 16 Laminar wake: temperatures along axis.

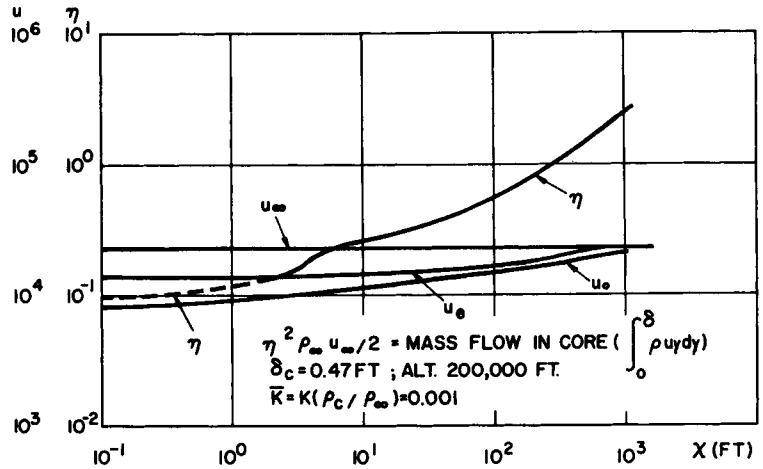

a. Velocities Along Axis, Outer Edge of Core, and Free-Stream, and Mass-Entrainment Parameter

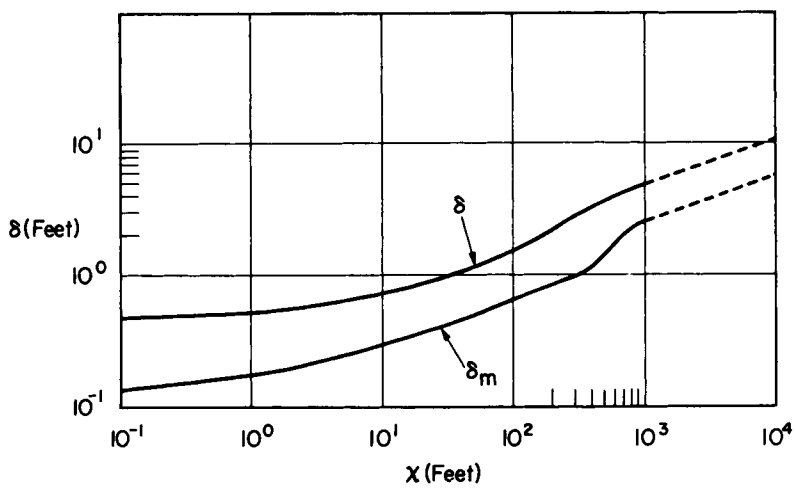

b. Transformed and Actual Core Thickness

Fig. 17 Properties of a turbulent core within a vortical shock induced outer flow.

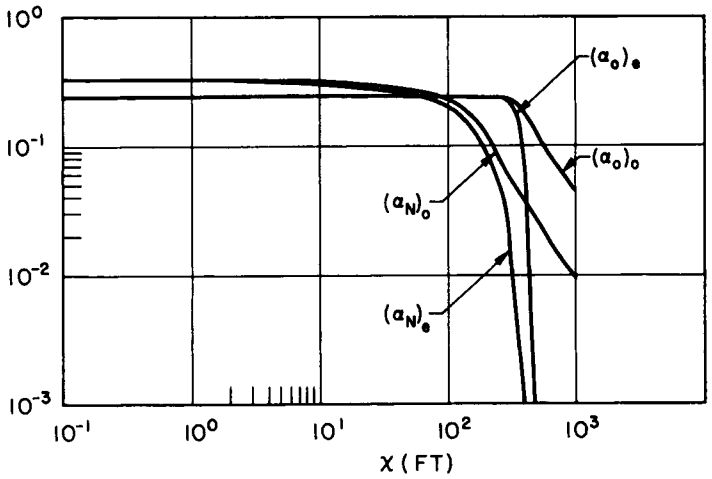

c. Atomic Mass-Fractions Along Axis and Edge of Core

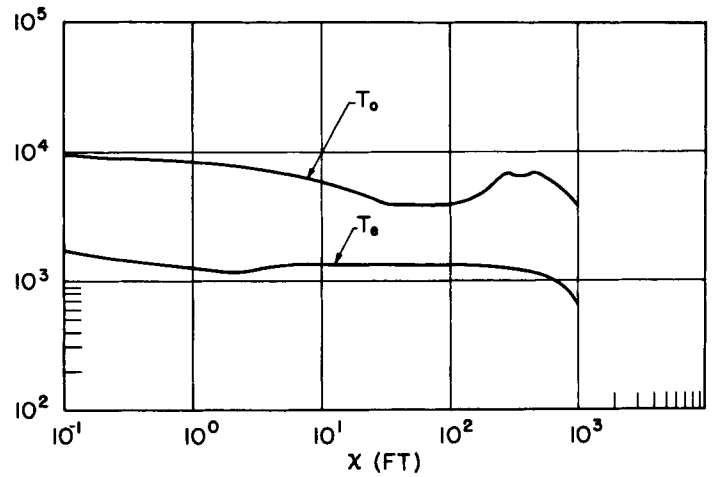

d. Temperatures Along Axis and Edge of Core

Fig. 17 cont'd. Properties of a turbulent core within a vortical shock induced outer flow.

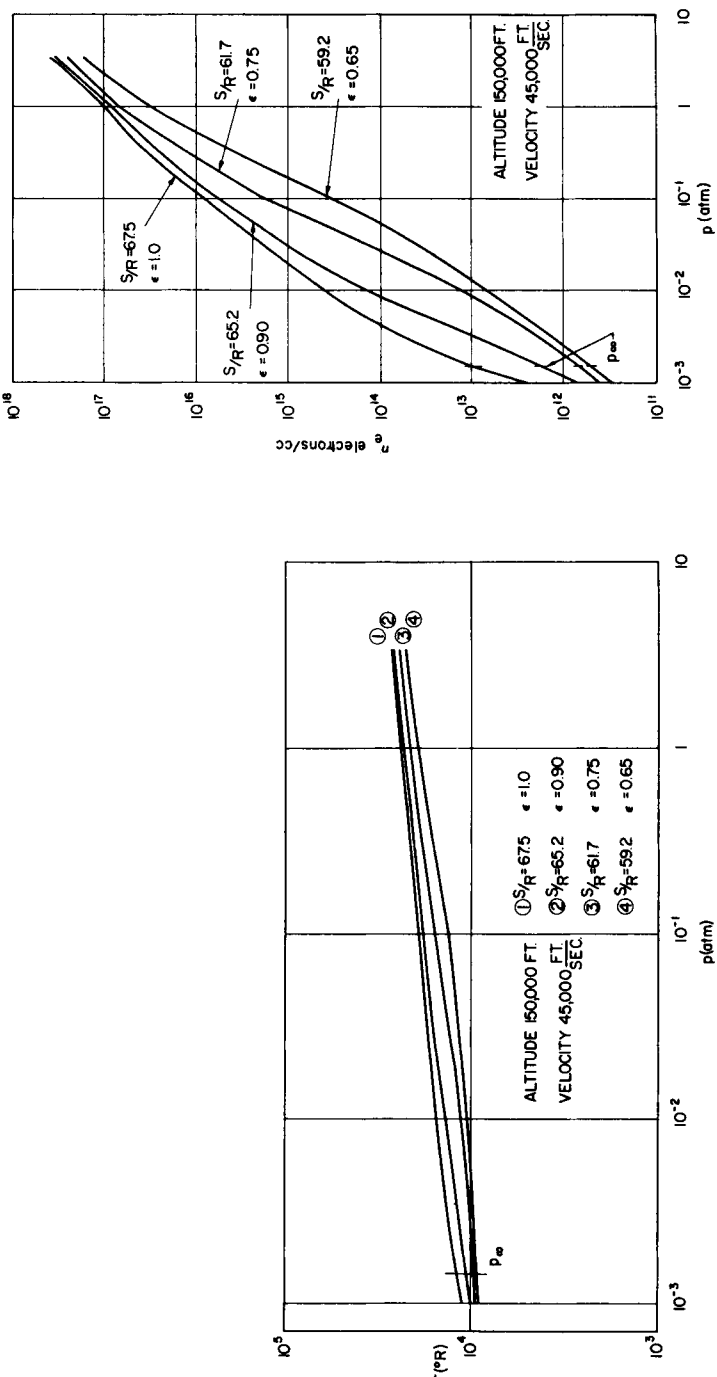

Fig. 18 Temperature and electron density distributions along streamlines in equilibrium with various amounts of initial heat loss by radiation. (ϵ is the remaining fraction of initial stagnation enthalpy.)